AN ABSTRACT OF THE THESIS OF

CHARLES MICHAEL ANDERSON for the DOCTOR OF PHILOSOPHY
(Name of student) (Degree)

in Mechanical Engineering presented on SEPT 11, 1973
(Major) (Date)

Title: INITIAL PERFORMANCE OF RIGID, POROUS SHEETS OF SINTERED-POLYETHYLENE POWDER FOR FILTERING AIRBORNE SANDER DUST

Redacted for privacy

Abstract approved: _____
R. W. Boubel

The mechanisms involved in the filtration of particulate matter by porous media are well established and reported in the literature. Estimates of the relative influence of each mechanism are determined by the use of various proposed dimensionless groups.

In this experiment the filtration of sander dust by means of rigid porous sheets of sintered-polyethylene powder is studied for various specified values of pore size (19 and 32 μm), filter velocity (15, 20 and 25 fpm) and mass loading (0.005, 0.01 and 0.015 gm/ft^3). A 2 x 3 x 3 factorial experiment with three replications was used.

The following primary conclusions were reached.

1. Pore size is significant with respect to penetration.

Filter	Pore size (μm)	Penetration
A	19	0.0066
C	32	0.0083

2. Neither filter velocity or mass loading is significant.
3. Direct interception appears to be the dominant filter mechanism.
4. Pressure drops are linear with filter velocity.
5. Pressure drop for filter A is 3.34 times greater than that for C at the same filter velocity.
6. With efficiencies greater than 99% for both filter pore sizes, it is questionable whether the 21% decrease in penetration would be worth the significant increase in power requirement.

Further experimentation is needed, especially in reducing experimental errors associated with the data.

Initial Performance of Rigid, Porous Sheets of Sintered-Polyethylene Powder for Filtering Airborne Sander Dust

by

Charles Michael Anderson

A THESIS

submitted to

Oregon State University

in partial fulfillment of
the requirements for the
degree of

Doctor of Philosophy

June 1974

APPROVED:

Redacted for privacy

Professor of Mechanical Engineering
in charge of major

Redacted for privacy

Head of Department of Mechanical Engineering

Redacted for privacy

Dean of Graduate School

Date thesis is presented SEPTEMBER 11, 1973

Typed by Ilene Anderton for Charles Michael Anderson

ACKNOWLEDGEMENTS

I wish to express my thanks to the members of my doctoral committee with regard to my graduate program. I especially appreciated the help offered by Dave Thomas associated with the statistical analysis and interpretation of the results.

The assistance offered by the following group of associates, friends and organizations is also appreciated: The U.S. Environmental Protection Agency for financial assistance under EPA grant number T 900047; the Porex Materials Corporation and the Nuclepore Corporation for supplying filter materials; the Weyerhaeuser Company for supplying sander dust samples and technical assistance; Wendy Moore and Frank Augustine for providing photo-micrographs, and Jack Kellogg, mechanical technician, for his invaluable patience and aid in helping me to acquire the skills necessary to fabricate the experimental apparatus.

My very special thanks are offered to Connie for being a special person and to Dick and Ruth Boubel for helping to make my experience at OSU thoroughly rewarding and enjoyable.

Doctoral Committee: R. W. Boubel, E. W. Hewson, J. G. Mingle, R. J. Schultz and D. R. Thomas.

TABLE OF CONTENTS

LIST OF FIGURES

LIST OF TABLES

NOMENCLATURE

List of Symbols

A	=	Area
A_d	=	Pore cross-sectional area
A_o	=	Filter cross-sectional area
b	=	Constant associated with orifice Reynolds number
C'	=	Orifice "constant"
C_s	=	Slip correction factor
d	=	Pore diameter and difference between means
D_c	=	Collector dia
D_p	=	Particle dia
F	=	Various orifice factors
f	=	Function
G	=	Gravity settling parameter based on collector size
g	=	Acceleration of gravity
h_w	=	Orifice differential pressure
I	=	Inertial impaction parameter based on collector size
K	=	Constant
k	=	Constant
Kn	=	Knudsen number
L	=	Pore length or filter thickness

N_G = Gravity settling parameter based on pore size

N_I = Inertial impaction parameter based on pore size

N_R = Direct interception parameter based on pore size

N_S = Sieving parameter based on pore size

P = Porousity

Δp = Differential pressure

p_b = Base pressure

p_f = Flowing pressure

p_o = Pressure at upstream filter surface

p_1 = Upstream absolute pressure

p_2 = Downstream absolute pressure

Q = Volumetric flow rate

Q_b = Volumetric flow rate at base conditions

Q'_b = Q_b when T_f = 110 F

Q_m = Volumetric flow rate at desired conditions

Q_o = Volumetric flow rate at upstream filter surface

R = Direct interception parameter based on collector size

Re_d = Reynolds number based on pore diameter

S_o = Specific surface area

Stk = Stokes number

T_b = Base temperature

T_f = Flowing temperature

T_o = Temperature at upstream filter surface

v = Velocity and filter velocity

v_o = Free-stream velocity

X = F_{pb}

Y = F_{tb}

Z = F_{tf}

α = Ratio of pore diameter to average distance between pores

η = Filtration efficiency

μ = Air viscosity

ϕ = Penetration

ρ_p = Particle density

ρ = Air density

Defined in Results

Nuc

Tube

Tot

Dimensional Units

C = Centigrade degree

cm = Centimeter

μm = Micrometer

cmHg = Centimeters of mercury

gm = Gram

μg = Microgram

F	=	Fahrenheit degree
ft	=	Foot
grain	=	Grain
in.	=	Inch
in. H_2O	=	Inches of water
in. Hg	=	Inches of mercury
Lbf	=	Pound force
Lbm	=	Pound mass
mil	=	Mil
min	=	Minute
sec	=	Second
cfm	=	Cubic feet per minute
fpm	=	Feet per minute
scf	=	Standard cubic feet
scfm	=	Standard cubic feet per minute

TERMINOLOGY

The following is a list of some of the terms used in this study which may not be in common use, or which may have more than one common meaning.

Average Pore Size: The size of filter pore which represents some average property of the pore distribution. In this study we refer to the mean-flow pore size unless specified otherwise.

Baghouse: An industrial gas cleaning device which removes suspended particles from gas streams using the mechanisms of fabric filtration. The particulate laden gas is drawn through the filter material by means of a blower. Although the filter material may be in one of many configurations, a bank of closed cylindrical tubes is often used.

Base Conditions: The desired conditions associated with volumetric flow rate in orifice calculations. Same as standard conditions in this study, where pressure is 14.7 psia [76 cm Hg] and temperature is 60 F (15.6 C).

Blinding: The continued internal buildup of particles in a filter with resulting reduced gas flow rates and possible failure.

Count Efficiency: Filtration efficiency based on the number (or count) of dust particles.

Cyclone: An industrial gas cleaning device which removes suspended particles from gas streams using centrifugal forces. The particulate ladened gas is drawn through the device by means of a blower. Centrifugal action of the gas causes the heavier particles to migrate toward the cyclone wall where they fall by gravitational forces to the bottom. Particles are discharged from the bottom and the carrier air passes up through the center of the device where it escapes through the top to the atmosphere.

Dust "Fall-Off": Dust originally collected on a vertical filter surface which falls off the filter due to gravitational forces either during or after the active filtration process. This dust does not pass through the filter but rather must be counted as a portion of the collected dust.

Filter Cake: The build up of collected dust on the surface of a filter. After sufficient time the cake becomes the primary filter medium.

Filter Velocity: The "average" gas velocity approaching a filter surface as found by dividing the total volumetric flow rate through the filter by the total filter cross-sectional area. It may be based on actual or standard conditions, and of course the terms should have consistent units. Also called superficial velocity.

Filtration Efficiency: The fraction of airborne particulate reaching a filter surface which is collected by that filter, on either a count or a mass basis, as found by subtracting the penetration from unity. It may be shown as a ratio or as a percentage. Unless specified otherwise, efficiency on a mass basis is to be assumed in this study.

Filter Performance: The effectiveness of a material in filtering a specific dust.

Geometric Deviation: A measure of dispersion for a log-normal distribution; the 84.13% value divided by the 50% value as observed from a cumulative frequency distribution.

Initial Filter Performance: Filter performance prior to the build up of filter cake.

Log-Normal Distribution: A statistical frequency distribution which is normal when plotted against the natural log of the variable.

Mass Efficiency: The filtration efficiency based on the mass (or weight) of the dust particles. Also called weight efficiency.

Mass Loading: The mass of a dust carried by a moving gas per unit volume of the gas. It may be based on actual or standard conditions. Also called solids loading or dust loading.

Mean-Flow Pore Size: The pore size such that when a fluid is forced through the filter medium under pressure, one-half of the fluid by volume passes through pores of equal or larger size, and

one-half passes through pores smaller in size.

Mean Particle Size: The median size particle of a dust with distributed size, based on count or mass, whichever is specified.

Monodisperse Size Distribution: A size distribution with values over a narrow range such that the sizes may be assumed to have a single, common value (homogeneous).

Nuclepore: A uniform high-efficiency, lightweight filter media produced by the Nuclepore Corporation using nuclear irradiation techniques. Used as the down-stream filter media in this study.

Particle Size: The "size" of a dust particle represented by the diameter of a circle whose area is the same as that of the actual particle as observed under a microscope.

Particulate: Any group of particles or dust carried by a gas stream.

Penetration: The fraction of airborne particulate reaching a filter surface which passes through the filter and is therefore not removed from the gas stream.

Polydisperse Size Distribution: A size distribution with values over a wide range such that a single value of size may not be assumed (heterogeneous).

Pore Size: The diameter of a pore of circular cross-section which is equivalent (with respect to characteristics related to surface tension effects) to the actual pore in question. Since the

actual pores are neither circular nor uniform, the "mean-flow pore size" will be useful as an average value.

Porex: A term used to specify the rigid, porous sintered-polyethylene powder filter material examined in this study and supplied by the Porex Materials Corporation.

Porosity: The ratio of pore volume to total (solid + void) filter volume.

Sinter: A process in which particles in contact with each other have their temperatures raised to just below the melting point. Bonds of sufficient strength to "hold" the particles together may be created in this way.

Size Distribution: The distribution of sizes, e.g., relative frequency distribution, of a group of objects with varying diameters. This term may refer to particles or pores in this report.

Standard Conditions: The condition where the pressure is 14.7 psia [76 cm Hg] and the temperature is 60 F (15.6 C).

INITIAL PERFORMANCE OF RIGID, POROUS SHEETS OF SINTERED-POLYETHYLENE POWDER FOR FILTERING AIRBORNE SANDER DUST

I. INTRODUCTION

The Problem

The production of plywood and particleboard involves a sanding process in which a thin layer of the sheet is removed to produce a smooth uniform surface. This process may generate a considerable amount of sander dust which must be removed, either for disposal, or preferably for some beneficial use, for example, as boiler fuel. Traditionally, the systems used to accomplish this bulk transfer of sander dust from the sanding area to a storage area have incorporated pneumatic conveyance principles. Although there are many specific systems in use, the major components often include the following:

1. Dust pickup hood at the sander
2. Fan
3. Pneumatic ducting
4. Large-diameter cyclone

The fan may be located between the sander and the cyclone, or downstream of both, the first case being perhaps more common. Here, the fan draws air at high velocities through the pickup system

so that the sander dust is drawn into the ductwork. It passes through the fan and is blown into the cyclone where centrifugal forces act to separate the sander dust from the air stream. The bulk of the dust is emitted from the bottom of the cyclone, and the carrier air is emitted from the air outlet, usually at the top. However, the cyclone is not 100% efficient, and a portion of the dust is released to the atmosphere along with the carrier air.

In the event that it is desired to reduce the percentage of dust emitted to the atmosphere (increase the system efficiency), it will be necessary to modify the system. One method would be to add another dust separator to the system, downstream of the cyclone air discharge, which is capable of removing sander dust from the cyclone discharge air with high efficiency. However, due to considerations of sander dust size distribution and cyclone removal mechanisms, the addition of a second cyclone in series with the first would not be especially effective, and other devices must be considered which are more effective at removing the "smaller" particles which are not collected by the cyclone. The industrial baghouse, which utilizes the principles of fabric filtration, has been successfully used in this application.

Another type of equipment used for this purpose functions in a manner similar to the baghouse, except that the filter media is rigid, porous sintered-polyethylene powder rather than fabric.

One industrial firm has developed a system using tubes of this material to filter the airborne sander dust, installed either as an integral part of the cyclone air exhaust, or as a separate component to be added to the existing cyclone air exhaust.

Although systems using the sintered-polyethylene powder filter material (hereafter called "Porex") have been installed on sander dust systems, the writer has been unable to find any significant studies attempting to relate Porex physical properties, and air and dust flow characteristics, to filtration efficiency. This will be the general subject considered herein.

Statement of Purpose

The primary purpose of this study is to determine whether or not pore size has a significant effect on the efficiency of Porex material used for filtering airborne sander dust.

Of secondary importance, the effects of varying filter velocity and dust mass loading will be studied. Since the cost of operating power is important, the effect of pore size on pressure drop will also be considered.

In conjunction with the specific purposes of this study, methods and operating procedures must be developed for the following:

1. Rapid and inexpensive determination of Porex pore size.

2. Accurate generation of very small, predetermined sander dust flow rates.
3. Support for the Porex filter material which allows easy access yet which maintains a high degree of integrity.
4. General experiment setup.

This study will consider only initial filtration performance and will not deal with the effects of filter cake buildup.

Preliminary Comments

There are some major difficulties in using sander dust to test filter performance. First, individual sander dust particles are not spheres but rather are highly irregular in shape, so that there are many possible definitions of particle size, or particle diameter, none of which represents the "true" size and shape. Second, sander dust is a polydisperse dust, so that some "average" size may not truly represent the dust particles as a group. Since any theoretical filtration equations will most likely assume monodisperse spherical particles, it may not be known whether deviations between theory and experiment are due to errors in the basic theory or to errors in particle description. This problem is multiplied when the filter pores are also of irregular shape and polydisperse in nature. Third, sander dust may contain many large particles which are highly susceptible to gravitational forces, with the result that under low

carrier gas flow rates some of the particles may settle out. Under these conditions the dust mass loading and size distribution will vary with distance upstream of the filter surface. All three of these conditions exist in this study.

The filters examined in this work are composed of tiny polyethylene "spheres" which are sintered to form a rigid, porous material, and are referred to in this study as Porex material. One fabrication technique involves laying out commercially procurred polyethylene powder on a suitable flat base in the form of a sheet by means of a doctoring blade, after which the sheet is passed through a furnace at a temperature just below the melting point. The points of contact between the powder "spheres" become bonded bridges, thus producing a rigid, porous sheet of polyethylene. Various thicknesses and pore sizes are available.

It must be realized that "pore size", or "pore diameter", does not necessarily indicate the physical dimension of the actual pores in the filter material. Furthermore, the actual pores do not approach a circular cross-section but are instead highly irregular in shape, and the pore size distribution is polydisperse with a wide range of values. Also, for thin material, where thickness is on the order of several times the powder diameter or less, average pore size will be related to thickness as well as to powder diameter, due to surface effects.

Finally, because of severe temperature limitations due primarily to the powder bonding mechanism, Porex-type filter material may be applied successfully only to systems where the carrier gas temperature (at the filter) does not greatly exceed ambient. Due largely to this requirement, Porex-type material has been applied most often to wood handling systems (sander dust, saw dust, bark dust, etc.) and, to some extent, to grain conveyance systems.

Limitations

There are certain limitations to the application of the results of this study to other situations.

1. The results may be applied only to those cases where operating conditions (temperature, pressure, etc.) are not significantly different from those used in the tests.
2. The results may be applied only to the ranges of values of filter velocities and mass loadings used in the tests.
3. The results may be applied only to polyethylene filter media with pore sizes, shapes and distributions similar to those tested.
4. The results may be applied only to fir sander dust, with size distributions similar to those tested. Specifically, the results may not be applied to the filtration of other

dusts with different sizes, size distributions, shapes or densities. This eliminates many sander dust systems which do not employ a cyclone pre-cleaner, since the size distribution may be different. Note: These dust properties are considered at the filter surface, not at the dust generator or some other point upstream of the filter surface.

5. The results are specifically applicable only to the case where dust build-up on the Porex surface does not exceed those values used in the study. This limits the results to initial filtration performance prior to any major filter cake buildup.

Comments on Dimensional Units

There is a complicated mixture of units in the various disciplines associated with the processes and applications of filtration, and it is not uncommon to see units of feet per minute and micrometers in the same report. Also, in the present report, available instrumentation resulted in data being recorded with such units as inches of water, grams, inches and micrometers. Consequently, the following procedure is used to try to reduce the seriousness of the problem.

1. All data are recorded in original (mixed) units.

2. All Figures and Tables use original units.

3. In the text, original units are used, followed in parentheses by their respective conversion to metric units.

4. A list of appropriate conversion factors is given below.

1 ft	=	30.5	cm
1 ft/min	=	0.508	cm/sec
1 ft^3/min	=	472.	cm^3/sec
1 gm/ft^3	=	3.53 $(10)^{-5}$	gm/cm^3
1 grain	=	0.0648	gm
1 $grain/ft^3$	=	2.29 $(10)^{-6}$	gm/cm^3
1 in.	=	2.54	cm
1 $in.^2$	=	6.45	cm^2
1 $in.^3$	=	16.4	cm^3
1 in. H_2O	=	0.187	cm Hg
1 $Lbf/in.^2$	=	5.17	cm Hg
1 Lbm	=	454.	gm
1 Lbm/ft^3	=	0.0160	gm/cm^3
1 Mil	=	0.076	cm
F	=	$32 + (\frac{9}{5})$ C	

II. LITERATURE REVIEW

History

According to an extensive report by the GCA Corporation (17) fabric filters were probably used during the Egyptian Old Kingdom (5000 BC) in the textile and metallurgical technologies developed during that time. The earliest recorded applications involved the use of fabric filters as masks to prevent inhalation of various occupational dusts, and the major stimulus to the development of filtration theory was based on the need for respiratory protection. Early systems which were the basis for modern industrial baghouse systems were developed in the nineteenth century primarily for fume control. Development and presentation of fabric filtration theories may be found in the GCA report, a report by the American Petroleum Institute (1) and a paper by Chen (12). The GCA and API reports also discuss filtration by media other than fabric. A bibliography of nearly 500 entries is listed with the GCA report alone (Volume III).

There is little evidence of any major interest in using sheets of sintered powder as filter elements prior to the second world war. Pall (31) indicates that sintered stainless steel filters were used for removing fluid catalyst fines in two fluid catalyst plants installed in 1953. Within the last decade Kane et al. (22) discuss the use of

sintered stainless steel powder for filtering dust from high-temperature coal-gasification processes, and Carls and Levitz (11) report on the use of sintered metal filters to remove entrained bed particles from pilotplant fluid-bed reactor effluent.

According to Clark (13) the first industrial application using sintered polyethylene powder for the filtration of sander dust was installed by Rader Pneumatic Company in the late 1960's. It must be pointed out that Rader has recently discontinued its line of WF-(sintered polyethylene) Filters primarily as a result of material blinding problems associated with the filtration of fibrous dusts. However, several of the Rader systems remain in satisfactory operation today, and a Los Angeles firm is using the polyethylene material for small-scale filter applications.

The mean pore size of the Rader WF-Filters is quite large, in some cases exceeding 100 μm, as shown by Boubel (9). It is possible that the use of smaller pore sizes could reduce or eliminate the blinding problem.

Sander Dust

Volume I of a report prepared for the Environmental Protection Agency by the Midwest Research Institute (28), lists the estimated U.S. production of plywood in 1968 as 15 billion ft^2 on a 3/8-in. basis, and states that approximately 45 dry tons of sander

dust is produced per million ft^2 of plywood manufactured and that roughly 10% of this will be emitted by cyclones to the atmosphere. The annual U.S. plywood sander dust emission rate as of 1968 was therefore about 67,000 tons per year, discharged from cyclones. Volume II of the MRI report (29) states that plywood sander dust from a drum sander has a mean count size of 22 μm (optical microscope measurement) and that Bahco analyses yield the cumulative size distribution, on a weight basis, presented in Table 1.

Table 1. Cumulative size distribution of plywood sander dust size on a weight basis by Bahco analysis.

Size (μm)	Cumulative weight (%)
5	5.2
10	18.0
20	35.5
40	93.1

This table shows, for example, that particles of 20 μm diameter or smaller comprise 35.5% of the weight of all particles. Care must be used when applying this data, however, since the report does not state whether the information applies to the dust before or after passing through a cyclone. Due to the relatively large count mean size, it is likely that the values are for pre-cyclone data.

Boubel (7, 8) has sampled several plywood plants for sander dust emissions. Pertinent data for the emissions from three sander dust cyclone sources are given in Table 2. The averages are roughly 4.5 μm count mean size and 0.12 grains/ft^3 mass loading.

Table 2. Sander dust cyclone emissions from three sources in Oregon (1971).

Exhaust temp (F)	Airflow (dry scfm)	Mass loading (grains/scf)	Count mean size (μm)	Geometric deviation
82	13,082	0.085	5.3	1.51
88	11,821	0.148	4.0	1.62
88	3,804	0.113	4.1	1.46

Isaacson (20) has supplied information regarding one of Weyerhaeuser Company's newer particleboard plants. The system utilizes multiple cyclones which discharge the carrier air to a baghouse. With a volumetric flow rate of 70,000 cfm [$33\ (10)^6$ cm^3/sec] and a dust mass flow rate of 250 Lbf/min [1880 gm/sec] from the sander, the mass loading to the cyclones is roughly 3 grain/ft^3 [$6.87\ (10)^{-6}$ gm/cm^3]. If the cyclone system is 90% efficient, the mass loading to the baghouse will be 0.3 grains/ft^3 [$6.87\ (10)^{-7}$ gm/cm^3]. Junge (21) has stated that the size distributions of plywood and particleboard sander dust are quite similar, and that cyclone sander dust from Weyerhaeuser installations have count

mean particle sizes ranging from about 3 to 15 μm, with a majority between 5 and 10 μm.

There are also some important considerations concerning the relationship between particle size distributions at various points of a system downstream of the cyclone air exhaust. This is especially important when some particles are larger than 5 to 10 μm. With regard to many common commercial filter systems, for example, baghouse-type design, the GCA report states that many of the larger particles may settle out without ever reaching the filter surface, due to reduced velocities within the device. This indicates that the size distribution of particles reaching the filter will be different from (skewed to the left of) the size distribution of the particles collected in the hopper of the device. In situations where this is true, there are two major consequences. First, the efficiency of the filter unit taken as a whole will be greater than the efficiency, based on the dust reaching its surface, of the filter material. Second, the performance of the filter material must be based on a smaller mean particle than that of the system as a whole. That is, the mean particle size of the dust reaching the filter material is smaller than that of the dust collected by the unit.

Particle Sizing

The MRI report, Volume III, (29) describes seven methods

used for determining particle size and size distribution. Microscopic analysis will be employed throughout this study; maximum resolution for a light microscope is about 0.5 μm. Cadle (10) discusses several particle-sizing techniques which require the use of a microscope, including the equal-area method employed in this study. The use of a porton-type graticule as a tool of this method is also discussed. The American Society for Testing and Materials (5) also covers this area, along with methods of sample preparation.

Dust Generation

Kraus (23, 24) discusses the various methods and considerations involved in pneumatic dispersal and conveyance of pre-formed (bulk) dust. Farnworth (15) made additional suggestions specifically with regard to a bulk sander dust feed mechanism. He suggested the possibilities of using a small scale screw feeder, a rotating metering valve, or a direct suction technique utilizing a hose with an adjustable exterior sleeve to provide intake air at depth in the dust bin. Although each of these methods has been used successfully in large-scale commercial applications, there are several formidable problems associated with accurate conveyance of very small quantities of bulk dust under predetermined conditions. For example, Holt and Young (19) indicate that any attempt to create airborne asbestos dust by blowing air through bulk dust would fail because

the fibers tend to cling together. This same problem exists with sander dust, and the result is a change in size distribution. In addition, the mass loading may vary greatly with time in a small-scale system.

Consequently, a dust generation system was developed which does not use bulk dust. A commercial belt sander was modified for this purpose.

Efficiency Test Methods

A detailed description of methods used in the U. S. for measuring the efficiency of filters appeared in the January 1962 issue of Heating, Piping and Air Conditioning (18), and May (27) compares the three methods now in common use. The AFI Weight Method requires a special synthetic dust, and efficiency is determined by gravimetric analysis. The upstream dust concentration is established by the weight of dust fed during the test period, and the downstream concentration is determined by measuring the weight of dust collected on a tared, sub-micron filter which must be at least 99% efficient with respect to the test dust. All of the air must pass through the downstream filter. The Dust Spot Method involves withdrawing samples of air upstream and downstream from the test filter. These samples are passed through chemical filter paper, and optical techniques are used to measure filter discoloration.

Efficiency is based on relative opacity. Either atmospheric dust or a special synthetic dust may be used. The DOP Method uses condensed dioctyl-phthalate droplets as the test dust, and concentrations upstream and downstream are measured using a light scattering device.

Due to considerations of dust size distribution, dust fall-out and optical characteristics, the Dust Spot and DOP Methods, which both involve light transmission measurements, are not suitable for the determination of mass efficiency for sander dust filtration situations. However, with modification, the AFI Weight Method should provide realistic efficiency data. First, due to dust fall-out, the upstream concentration must be determined at the face of the filter surface. Second, it may be necessary to collect the dust deposited on the tube section between the test filter and the downstream filter.

Strauss (45) has compared both U. S. and European techniques. He concluded that, in addition to specifying the test method completely, complete assessment of a filter medium requires knowledge about clean filter resistance, dust removal efficiency and the effects of dust accumulation on both resistance and efficiency.

The Filter Material

The writer has been unable to find any published articles in the

literature dealing specifically with rigid, porous filter materials formed by sintering polyethylene powder, referred to here as Porex material. However, technical data is available from two firms which produce the material commercially, Porex Materials Corporation (33), supplier of the porex material used in this study, and Porvair Limited (34).

POR·X, trademark of Porex Materials Corporation, identifies a permeable thermoplastic product with omni-directional, interconnecting pores. This general product may be produced from many different plastics utilizing several different techniques, and is available in many different sizes, shapes and porousities. The material examined in this study is formed in sheets by sintering linear (high density) polyethylene powder. Within limits, filter thickness and pore size can be varied to specified values. A predetermined thickness is relatively simple to obtain by adjusting the height of the doctoring blade and applying a post-sinter pressure process. Predetermining pore size is somewhat more difficult.

Literature on the high-efficiency filters which are positioned downstream of the test filters may be obtained from the Nuclepore Corporation (30). Spurny et al. (44) consider Nuclepore structural and filtration properties. Nuclepore filters are membrane filters with uniform, straight through, circular pores. Standard pore sizes range from 0.1 to 8 μm in diameter with tolerances of +0 and

-10 percent. Thickness is only 10 μm so that a very small tare weight of just over 1 mg/cm^2 results.

Pore Size Determination

The American Society for Testing and Materials (3) has published a standard method of test for the determination of maximum pore diameter in rigid porous filters, E 128, in which the filter is immersed in a suitable test liquid and air pressure is applied until the first bubble passes through the filter. The maximum pore diameter is calculated from the surface tension of the test liquid and the applied pressure. Although this method is relatively simple and inexpensive, it has a major drawback in that it does not provide information about the average pore size or about the pore size distribution.

Rootare (37) presents a review of mercury porosimetry as a method of measuring pore size distributions in porous materials and also discusses possible sources of errors. It is a well established method of measuring pore-size distribution in porous solids and will also yield information about average pore size. However, specialized equipment is required.

Anderson (6) describes a method used by the Association of American Railroads for testing fuel filters which specifies a procedure for determining mean-flow pore size and pore size

distribution based partly on the same principles applied in ASTM: E 128. The ASTM (4) specifies a similar procedure for testing membrane filters for use with aerospace fluids, ASTM Tentative Method of Test: D 2499. These methods require two sets of data. First, using a dry filter, volume flow rate is plotted against pressure drop across the filter. Second, the filter is wetted with an appropriate liquid which has a known surface tension, and volume flow rate is again plotted against pressure drop. The bubble pressure for the mean-flow pore is determined by locating the pressure drop at which the wet flow rate is one-half of the dry flow rate. The mean-flow pore size is then calculated from the capillary rise formula based on surface tension effects which is derived in Appendix A as in ASTM: E 128.

ASTM: D 2499 gives a procedure for determining the pore size distribution on a percent flow basis; that is, the percentage of the total flow passing through a range of pore sizes, with specified upper and lower limits, may be determined.

Anderson suggests that, at least for membrane filters, correlation between the results of this method and the mercury intrusion method is very close. He also states that high grade diesel fuel has been used as a wetting fluid by the AAR for all types of bubble pressure testing. It has proved to be better than the alcohols for this purpose and has been found to be very satisfactory. ASTM:

D 2499 specifies mineral oil, such as USP Liquid Petrolatum Heavy.

The basic procedure described above for determining mean-flow pore size is used in this study in attempting to verify mercury porosimetry data supplied by Porex Materials Corporation. Aviation jet fuel is used as the wetting liquid.

However, care must be exercised as pointed out by Scheidegger (38). He cautions that the capillary model from which all capillary rise equations are derived is a far cry from most real porous media so that at best the results will give only a good qualitative indication of pore size and size distribution.

Filtration

The GCA report (17) provides a description of the various stages of fabric filtration which should apply at least qualitatively to filtration by Porex-type material. The initial phase begins with the capture of individual particles by single fibers (collectors) within the flow field. These collected particles protrude into the flow field and act as additional obstacles for future capture of particles. In this manner, chain-like deposits accumulate on the individual fibers, and bridges across the flow channels begin to form. Observation of aggregate structures shows that deposition occurs primarily on previously deposited particles rather than on bare fibers, indicating an increase in filtration efficiency with

increased particle deposition. As the process continues a more or less continuous deposit of accumulated material forms having the appearance of a uniform cake. Filter cake is the name given to this material which is accumulated primarily on the surface of the filter, although some deposition does take place in the body of the filter, especially during the initial phase of filtration. Pressure drop rises during filter cake buildup due to a combination of smaller channels and more obstacles in the flow field, resulting in a decrease in total flow below some desired value. The accumulated dust is then removed from the fabric by stopping the flow and vigorously shaking the element, or by on-line reverse-air or jet cleaning. Although a large amount of the dust is removed in this process, a substantial amount still remains within the inter-fiber spaces. Complete, or nearly complete cleaning is possible, although it is usually not economical, or even desirable, since efficiency will be reduced during the build up of the new cake. For fabrics, the pressure drop ratio just prior to cleaning is on the order of 200:1, and just after cleaning it is on the order of 100:1. Pressure drop ratio is defined as the ratio of existing filtering pressure drop to clean-filter pressure drop.

The American Petroleum Institute (1) recognized seven primary mechanisms which may play a part in any filtration process. These mechanisms are described in Table 3. In addition, Davies

Table 3. Primary filtration mechanisms.

1.	Direct sieving occurs when the particles are larger than the pores of the filter.
2.	Direct interception occurs when a fluid streamline passes close enough to the filter media that a particle following that streamline touches the filter.
3.	Inertial impaction occurs when the mass of a particle is so great that the particle crosses streamlines which are bending around the filter and is intercepted.
4.	Brownian diffusion causes interception to occur due to the random motion of very small particles superimposed upon the bulk fluid motion.
5.	Gravity settling causes interception to occur due to increased relative vertical motion caused by the earth's gravitational field.
6.	Electrostatic precipitation causes interception to occur due to electrostatic forces which may exist between the filter and the dust particles.
7.	Thermal precipitation causes interception to occur due to a thermal gradient which may exist between the gas stream and the filter surface.

(14) suggests that molecular forces may influence deposition to some small extent when the distance between a particle and the filtration surface is small. It should be clear that these mechanisms may operate whenever any obstacle is in the flow path, regardless of whether it is the actual filter surface of some other object, for example a dust particle, attached to the filter surface.

Fortunately, as the API report points out, it is not common for all of these mechanisms to have an appreciable effect in a single given filter situation. Often only one or two mechanisms will be in effect, and it is necessary to analyze each situation to determine which are present. We may rule out the mechanisms of thermal precipitation because strong thermal gradients would be required. Also, the influence of molecular forces will not be considered. Table 4, which is taken from the API report, offers a general guide to situations where the various mechanisms may be important. However, it must be noted that this summary is based on only one variable, particle size, and should therefore not be considered to apply strictly in all cases.

It is shown in the body of this report that the test dust size distribution is roughly log-normally distributed with a count mean of approximately 8.7 μm and a geometric deviation of 1.80. Thus, fewer than 20% of the particles are smaller than 5 μm and fewer than 1% are smaller than 2 μm. Furthermore, if we assume weight

to be proportional to the cube of size, as with a sphere, fewer than 0.5% of the particles by weight are smaller than 5 μm. Therefore, the effects of Brownian diffusion and electrostatic precipitation will be neglected on the basis of the information in Table 4. However, some static charge buildup was noted and the possible effects of this mechanism should be considered more thoroughly in future tests.

Four significant filtration removal mechanisms remain to be considered: sieving, direct interception, inertial impaction and gravity settling. Although this study will not attempt to specifically relate each individual mechanism to filter efficiency, it is useful to consider how the variables mass loading and filter velocity might influence each mechanism. This may yield some insight into the relationship between these variables and filter efficiency.

Table 4. Important particle sizes related to various filtration mechanisms.

Mechanism	Size range of importance (μm)
Sieving	> Filter Pore Size
Direct Interception	> 1
Inertial Impaction	> 1
Brownian Diffusion	< 0.01 to 0.05
Gravity Settling	> 1
Electrostatic Precipitation	< 0.01 to 5

The literature dealing with relationships between mass loading and filtration efficiency is quite misleading and caution must be used

in interpretation. For example, First and Silverman (16) state that collection efficiency improves markedly with increasing dust (mass) loading because high dust loadings lead to very rapid accumulation of the high efficiency filter cake while low dust loadings result in prolonged periods of less efficient media filtration. The statement here should be that efficiency increases with total dust collected, not specifically with dust loading. That is, if we consider only the reasoning cited, the instantaneous efficiencies of two systems which are identical except for different values of mass loading would be the same when both filters have collected the same amount of dust. Of course, if both systems begin operation at the same time, the system with higher mass loading will have a higher efficiency at a specified instant, but only because more dust has been collected at that instant. Thus, mass loading, independent of total dust collected, is not shown to influence efficiency. Volume I of the GCA report also indicates that increasing mass loading increases efficiency. However, the description is not complete and it is not clear whether the result is due to increased mass loading or total dust collected. Kane et al. (22) consider the individual effects of mass loading and total dust collected in their study of porous stainless steel filters. Although the figures used to present their data appear to show a relationship between efficiency and mass loading, the authors claim that the variations due to mass loading are not significant. Since an attempt

will be made to collect the same amount of total dust during each test in this study regardless of the value of mass loading, it will be possible to examine the influence of mass loading on efficiency.

There is a large volume of literature which attempts to relate filter velocity and collector or pore size to collection efficiency and to the individual mechanisms of filtration, especially in the area of fabric filtration. The bulk of this literature describes filtration in terms of the ability of individual obstacles (collectors) such as cylinders or spheres, when placed in a moving air stream, to collect particles carried by that air stream. See, for example, the API report (1), the GCA report (17) and Chen (12). In virtually all cases, dust particles and collectors are each considered to be of a single uniform size and shape. Parameters are then defined for each filtration mechanism, such that large values indicate high collection efficiency by that mechanism and small values ($<< 1$) indicate that the specific mechanism is not an important factor and may be neglected. The efficiency of collection by the obstacle is then defined as the ratio of the cross-sectional area of fluid stream from which all particles are removed to the projected cross-sectional area of the obstacle, and is a function of filtration mechanism parameter and in some cases Reynolds Number. The filtration efficiency of a filter is then considered as the total of the efficiencies of the individual obstacles, with the effect of neighboring obstacles corrected

empirically. It is to be expected that this technique will be less successful with close-packed spheres such as in Porex-type materials, than with fiber-type filters or fluidized-bed filters where inter-particle distances are greater. Finally, the effect of several mechanisms acting simultaneously is considered, often at least semi-empirically. It must be emphasized that the individual mechanism efficiencies are not necessarily directly additive because many of the airborne dust particles will be operated on simultaneously by more than one mechanism. Consequently, the total efficiency should be at least as great as the individually largest efficiency but usually less than the sum of all individual efficiencies.

It appears that Ranz and Wong (36) were the first to suggest the use of dimensionless parameters to determine the relative importance of individual filtration mechanisms. They applied the parameters to spherical dust particles and both cylindrical and spherical collectors. Note that a sieving parameter cannot be defined for a single individual obstacle; instead, it is seen that efficiency due to sieving will be 100% when particle diameter is greater than or equal to filter pore size, and zero otherwise. In any event, it is clear that collection by sieving is not a function of velocity or mass loading, but will be a function of collector size in those cases where pore size is related to collector size, as in the case of Porex-type materials.

The filtration parameters associated with the remaining mechanisms of interest in this study are given below as defined by Ranz and Wong and further discussed by API, GCA and Chen, among others.

Direct interception parameter: The ratio of particle diameter to collector diameter. While this mechanism may act independently, it must also be treated as a boundary condition for the other mechanisms.

$$R = \frac{D_p}{D_c}$$

Inertial impaction parameter: The ratio of the stopping distance of a particle with diameter D_p, density ρ_p and initial velocity v_o, to the diameter of the collector.

$$I = \frac{C_s \rho_p D_p^2 V_o}{18 \mu D_c}$$

Gravitational settling parameter: The ratio of free settling velocity of the particle to the free-stream velocity.

$$G = \frac{C_s \rho_p g D_p^2}{18 \mu v_o}$$

Where:

D_p = particle diameter (spherical equivalent)

D_c = collector diameter (spherical equivalent)

ρ_p = particle density

μ = carrier gas viscousity

v_o = free-stream velocity

C_s = slip correction factor for small particles; $\simeq 1$ here

g = local acceleration of gravity.

To obtain rough values of these parameters, use the following data. Calculations are performed in Appendix B.

D_p = mass mean particle size = 22 μm [$22(10)^{4}$cm] or

= count mean particle size = 8 μm [$8(10)^{4}$cm]

D_c = 40 and 70 μm [$40(10)^{4}$ and $70(10)^{4}$cm]

ρ_p = 0.625 gm/cm^3

μ = 0.448 Lbm/hr-ft [$185(10)^{-6}$ gm/sec-cm]

v_o = 15 and 25 ft/min [7.6 and 12.7 cm/sec]

C_s = 1

g = 32.2 ft/sec^2 [980 cm/sec^2]

Results are shown in Table 5.

If the values of the parameters do in fact indicate the effectiveness of the various mechanisms, it is clear that for dust particles of mean size on a mass basis, filtration is primarily due to inertial impaction. In general, efficiency should thus be a function of the parameter, I, and the Reynolds number based on collector size, Re_c. However, for low velocity viscous flow the dependence on Re_c is

negligible. To account for the effect of neighboring collectors it is likely that efficiency will also be a function of average distance between collectors.

Table 5. Values of filtration mechanism parameters based on collector size.

Parameter	Average value based on a particle size of	
	8 μm	22 μm
R	0.17	0.43
I	0.22	1.7
G	0.013	0.09

Spurney and Pich (42, 43) describe a filtration model for membrane filters using parameters similar to those considered above which may more accurately represent the case of filtration by Porex-type material. The model is based on surface rather than body filtration where the fluid flow is through capillary pores and the parameters are functions of filter pore size (diameter) rather than collector diameter. Pich (32) and Spurny and Lodge (41) discuss the model in further detail.

The parameters for the four mechanisms under consideration are given below. Note the close similarity to those cited above for the collector model.

Sieving parameter:

$$N_S = \frac{D_p}{d}$$

Direct interception parameter:

$$N_R = N_s = \frac{D_p}{d}$$

Inertial impaction parameter (Stokes number):

$$N_R = Stk = \left[\frac{2}{P}\right]\left[\frac{\rho_p D_p^2 v_o}{18\,\mu d}\right] = \frac{\rho_p D_p^2 v_o}{9\,\mu d P}$$

Gravitational settling parameter:

$$N_G = \left[\frac{3LP}{d}\right]\left[\frac{\rho_p g D_p^2}{18\,\mu v_o}\right] = \frac{LP\,\rho_p g D_p^2}{6\,\mu d\, v_o}$$

Where new symbols are

d = pore diameter

P = porousity

L = pore length = filter thickness

Rough values of the parameters may be obtained as shown in Table 6, where the following additional data are employed. Calculations are performed in Appendix B.

d = 19 and 32 μm

P = 0.4

L = 30 mils (0.076 cm)

Although not defined here, the parameter for diffusion is << 1, thus verifying our earlier decision to neglect this mechanism.

Table 6. Values of filtration mechanism parameters based on pore size.

Parameter	Average value based on a particle size of	
	8 μm	22 μm
$N_S = N_R$	0.36	0.94
N_I	3.2	20.
N_G	0.60	3.8

Although the relative importance of gravitational settling has increased under this model, it is clear that inertial impaction remains as the dominant filtration mechanism. If inertia is considered as the only collection mechanism, the model predicts that filter efficiency will be a function of the inertial impaction parameter, N_I, and the ratio of pore diameter to average distance between adjacent pores, α. However, it is easily shown that, for various theoretical methods of packing spheres, both pore diameter and distance between pores are linear functions of collector (sphere) diameter. See Appendix C. Since Porex-type material may be described roughly as a system of packed spheres it might therefore be expected that the ratio α would not vary substantially for filters of

various pore sizes, especially where the variation in pore size is not large. In this case, it would be expected that collection efficiency is a function of N_I alone.

Note that the model is based on efficiency on a count basis. If the dust particles are monodisperse, mass efficiency and count efficiency will be the same. However, for polydisperse dust particles collected primarily by the mechanism of inertial impaction, we expect mass efficiency to be greater than count efficiency. Nevertheless, mass efficiency will still be a function (but a different function) of N_I alone.

The following is a list of the major assumptions employed in the above model.

1. Filter pores are straight-tube capillaries of a single circular cross-section and with sharp-edge entrances.
2. Filter pores are geometrically placed at the center of hexagonal polygons visualized on the filter surface.
3. Streamline flow exists upstream of the filter surface.
4. Dust particles are monodisperse spheres.

None of these assumptions is correct in the present situation and it is expected that any theoretical equation for efficiency will deviate from experimental data. In particular, it was noted during flow calibration that velocity fluctuations exist and this turbulence may have some effect on collection efficiency. However, it is not unreasonable to expect the basic equation for efficiency, $\eta = f(N_I)$, to retain its validity. One encouraging feature is that the model accurately predicts

collection by membrane filters as a surface rather than body mechanism when N_I is large. Quackenbush (35), using microscopy techniques, has shown that filtration of sander dust by Porex-type material is also primarily a surface effect. Initial filtration by most fabric filters is somewhat more dependent on body mechanisms.

There is very little information available specifically on filtration by materials composed of sintered powder. D. B. Pall (31) has studied the filtration of fluid catalyst fines from effluent gases using filters of sintered stainless steel powder. Although he considers pressure drop in some detail he gives no specific information on efficiency. He used filters with a mean pore diameter of 20 μm (roughly 10 μm < d < 40 μm) and the dust particles ranged from 0.5 to 80 μm with a mean mass diameter of 40 μm. Consequently, one would expect very high efficiencies under the filtration model of Spurny and Pich. It is unfortunate that no filter data were given for verification. Kane et al. (22) also consider sintered stainless steel powder for filtering hot gases. Although specific data on efficiency is given in the form of plotted curves, there is not sufficient information to determine the relationship between efficiency and filter velocity. However, it is clear that efficiency increases with decreasing pore size as expected. Finally, Carls and Levits (11) consider sintered stainless steel powder for filtering entrained bed particles from fluidized bed gas effluent. However, they deal

specifically with the problem of blowback, a technique used to remove a portion of accumulated filter cake, and very little information of direct benefit to this study is presented.

Since Nuclepore filters are used in this study as the downstream high-efficiency filters, it will be useful to understand their ability to collect small particulate. According to a theory described by Spurny and Lodge (40) and Spurny et al. (44) and refined by Spurny and Madelaine (39), Nuclepore filters with pore diameters of 3 μm and porosities of 15% will have efficiencies of approximately 90% on 1 μm diameter sander dust particles in the range of filter velocities used in the present study. This calculation is presented in Appendix D. Since the inertial impaction mechanism is dominant in this situation we expect efficiency to increase for larger particles and decrease for smaller particles. Consequently, if for example the particle dust distribution has a count mean size of 1 μm or larger, we expect the mass efficiency of the Nuclepore filters to exceed 90%. This implies that if we measure a Porex filter efficiency of say 99%, the true value should be 98.9% if the Nuclepore efficiency is 90%.

Filter Pressure Drop

Scheidegger (38) considers several equations which relate volumetric flow rate and pressure drop for various flow conditions. For laminar flow in straight tubes the familiar Hagen-Poiseuille

equation applies so long as slip flow can be neglected.

$$Q = \left[\frac{\pi d^4}{128 \mu L}\right] \Delta p = \left[\frac{A_d d^2}{128 \mu L}\right] \Delta p$$

Where:

Q = Volumetric flow rate

d = Pore diameter

L = Pore length

μ = Fluid viscosity

Δp = Pressure drop across the pore

A_d = Pore cross-sectional area

Slip flow may be neglected when the Knudsen Number ($Kn = \frac{\ell}{d}$) $<< 1$, where ℓ is the fluid mean free path. For a pore diameter of 20 μm and air at standard conditions $Kn \simeq 0.01$ which we will assume to be sufficiently small to neglect the effects of slip flow.

For laminar flow through porous media the Darcy flow equation applies.

$$Q = -\left[\frac{k_1 A}{\mu L}\right] \Delta p$$

Where:

k_1 = Constant of the porous media

A = Cross-sectional area of the porous media (solid + pores)

There have been many attempts to determine k_1, the most common being the Kozeny-Carmen relationship.

$$k_1 = \frac{P^3}{K_1 S_o^2 (1 - P)^2}$$

Where:

K_1 = Constant

P = Porousity

S_o = Specific surface area

Machacova et al. (26) describe a relationship for flow through membrane and Nuclepore filters.

$$\Delta p = p_1 - \left[p_1^2 - \frac{K_2 \mu L v_o p_1}{P d^2} \right]^{1/2}$$

Where:

p_1 = Upstream absolute pressure

K_2 = Constant

v_o = Free stream velocity

However, it is easy to show (see Appendix E) that for the case $\Delta p << p_1$ this equation reduces to

$$Q = \left[\frac{A P d^2}{2 K_2 \mu L} \right] \Delta p = \left[\frac{K_3 A}{\mu L} \right] \Delta p$$

Notice the similarity between this and the previous equations due to Darcy and Hagen-Poiseuille.

Although Scheidegger cautions against the general acceptance

of equations based on cylindrical-pore theory for flow through porous materials, it is clear that for viscous flow through porous media we should expect Darcy's law to hold. However, it is not clear that the Kozeny-Carmen relationship is accurate. In any event, we expect volumeteric flow rate to be a linear function of pressure drop.

$$Q = \left[\frac{k\,A}{\mu\,L}\right] \Delta p$$

Although Reynolds number is not an accurate indicator of transition from laminar to turbulent flow in other than straight tubes, it is evident that viscous flow will exist in porous media for Re_d less than about 1, where $Re_d = \frac{\rho\, dv}{\mu}$. In the present study the largest average value is obtained for v = 25 ft/min [12. 7 cm/sec] and d = 32 μm, where $Re_d = 0.26$.

III. EXPERIMENTAL PROGRAM

Objective

The general objective of the experimental program was to investigate the initial performance of rigid porous sheets of polyethylene powder for filtering airborne sander dust. Within this broad area were the following more specific objectives:

1. To investigate the effect on initial filtration efficiency of three independent variables:
   a. Filter pore size
   b. Dust mass loading
   c. Fluid filter velocity
2. To investigate the effect of filter pore size and filter velocity on pressure drop.

Filter Properties

The original test scheme called for three grades of the Porex material, all with a thickness of 30 mils [0.076 cm]. The average pore sizes specified were 10, 40 and 70 μm. However, as stated earlier, it is a time-consuming (thus, expensive) process to produce material of a specified thickness and pore size which is new to the manufacturer. Consequently, the Porex material received for testing

varied in average pore size from roughly 15 to 45 μm, with most in the ranges from 18 to 22 μm and from 30 to 37 μm. There were only a few in the central range from 22 to 30 μm or in the high-end range from 37 to 45 μm. The filters were individually tested to establish the pressure drop for each at a filter velocity of 25 ft/min [12.7 cm/sec] so that filters of uniform quality could be selected. From these tests it was concluded that there were insufficient filters of the desired sizes and it was decided to use only two sizes rather than three. The first "group" was selected between 2.4 and 2.6 in. H_2O [0.448 and 0.486 cm Hg] and the second between 0.75 and 0.80 in. H_2O [0.14 and 0.15 cm Hg]. A sample from each was returned to Porex Materials Corporation for size analyses using the mercury intrusion technique (Aminco-Winslow Porosimeter Model 5-7118). Table 7 lists these results, along with thickness measurements, where the filters with smaller average pore size are designated as "A" and the larger as "C". It should be noted that the distributions of pore size were very irregular.

Table 7. Porex filter properties.

Filter	Porosity (%)	Average pore size (μm)	Range in pore size (μm)	Thickness (mils)
A	40	19	0 - 67	31
C	40	32	0 - 85	30

Several attempts were made to verify these values of average pore size using the mean-flow technique described earlier in the literature review. However, the values obtained were consistently determined to be lower (12 and 20 μm) than those in Table 7. Since the mercury intrusion technique has been established in the industry, and since no single number can truly represent the actual sizes and shapes of the pores, the specific measurement technique (based on the capillary rise model) may not be too important as long as it is used consistently, so the values in Table 7 will be used throughout this study.

Thickness measurements were made with a micrometer and checked using microscopy techniques. A value of 31 mils [0.078 cm] is accurate for Group "A", 30 mils [0.076 cm] for group "C". These values are included in Table 7. For simplicity, a value of 30 mils [0.076 cm] will be assumed for both groups in all calculations.

The overall quality varied significantly across the range of average pore size. In some cases filters seemed to be quite uniform, in others large voids or sections of solid volume appeared. Only those filters which appeared to have a uniform quality were used.

Prior to testing, each filter was vacuum cleaned to remove all foreign materials.

Sander Dust Properties

Although the purpose of this study was to consider the filtration of plywood sander dust specifically, blocks of fir 2 x 4's rather than plywood were used in generating the dust for two primary reasons. First, and most important, adjacent plywood veneers are oriented perpendicular to each other. Consequently, if the sander dust generator were to sand through consecutive layers, it is likely that some change in the dust size distribution would result. Second, 2 x 4 blocks were much easier to adapt to the dust generator for satisfactory results.

Accurate determination of the density of sander dust particles is quite difficult and it was finally decided to use the wood block density as an approximation. An attempt was made to measure the true particle density using volume-displacement vs. pressure techniques; however, densities of between 1.16 and 1.26 gm/cm^3 were obtained. It is likely that these high values are a result of excluding intra-particle void volumes from the density calculations. Conversely, wood block densities may be too low an estimate due to the inclusion of inter-particle void volumes in those density calculations. In any event, the dust particle density will be approximated by the measured block density, which in this study was determined to be 0.625 gm/cm^3. It must be realized that plywood densities are roughly 15% lower than this value, due primarily to a lower moisture content, and this fact must be considered when applying the results.

Samples of sander dust were collected on a filter at the Porex test section over the range of applied mass loadings and filter velocities used in the test. Although there were some minor differences between samples, they all plotted roughly as a log-normal distribution with a count mean of 8.7 μm and a geometric deviation of 1.8, with a resultant weight mean of 22 μm. See Appendix F. All particle sizing was done using light microscopy techniques. Slides were prepared by scraping collected sander dust particles into a jar of methyl alcohol, shaking vigorously, applying a drop to the slide and allowing the alcohol to evaporate.

A sample of sander dust was also taken from the collector bin of a commercial baghouse installation located downstream of a sander dust cyclone. A size analysis of this dust yielded a count mean of 9.8 μm and a geometric deviation of 1.94.

Table 8 summarizes the relevant properties of sander dust used in this study. Figures 1 and 2 are micrographs showing samples of the test dust and industrial dust, respectively. The scale of size is for reference only and is not meant to represent either an average or typical particle.

Table 8. Test sander dust properties.

Density	0.625 gm/cm^3
Size Distribution	Log-Normal (Approx.)
Count Mean Size	8.7 μm
Weight Mean Size	22 μm
Geometric Deviation	1.8

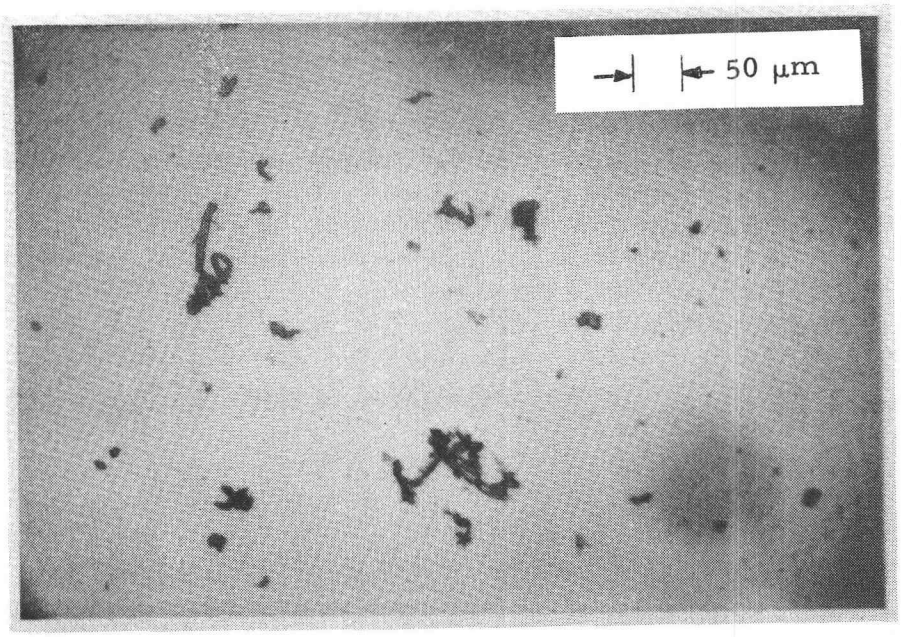

Figure 1. Test sander dust.

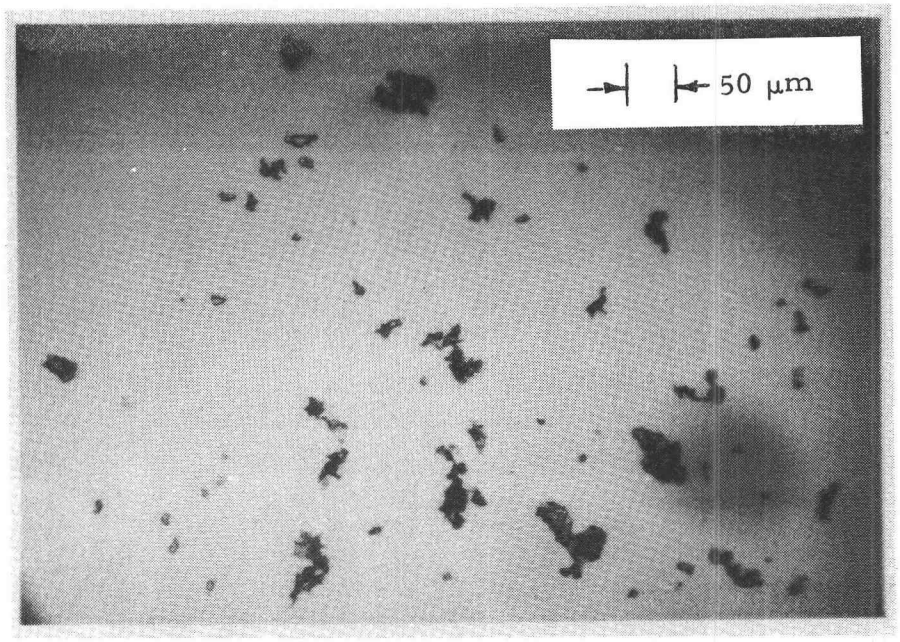

Figure 2. Industrial baghouse sander dust.

Equipment Description

In order to meet the project objectives, experimental equipment was either procured or designed and constructed according to the following criteria.

1. A sander dust generator must be constructed which provides dust at the filter test section of specified size distribution and uniform mass flow rate over a specified range of volume flow rates. This system must be enclosed and vented to the building outlet ventilation system.
2. A filter test section and adjoining flow sections must be built with the following characteristics.
    a. The closure mechanism must allow rapid insertion and removal of the test filter.
    b. The closure mechanism must provide a leak-proof seal for the test filter.
    c. A means of visual observation of the upstream face of the test filter during test runs must be provided.
    d. The upstream pressure must remain close to ambient through all values of test variables.
    e. A means of measuring pressure drop across the test filter must be provided.

f. The design must provide for uniform collection of dust on the filter surface.

g. The upstream flow section must allow ease of cleaning for gross removal of dust particles between tests.

h. The downstream flow section must allow ease in washing for fine removal of dust particles from the tube wall after each test run.

i. A means of calibrating filter dust retention (or fall-off) must be provided.

j. A means of calibrating face velocity and flow rate must be provided.

3. A downstream (Nuclepore) filter holder must be constructed which provides easy access for rapid installation and removal, and a leak-tight seal, for 90 mm filters.

4. A system of valves to accurately regulate the volumetric flow rate through the test section must be provided.

5. A vacuum pump must be provided to draw the required volumetric flow rates through the system.

6. A flow measuring device to indicate volumetric flow rates through the test section must be provided.

In addition, supplemental equipment such as a sensitive balance and laboratory oven must be available.

A schematic diagram of the system is shown in Figure 3 and a

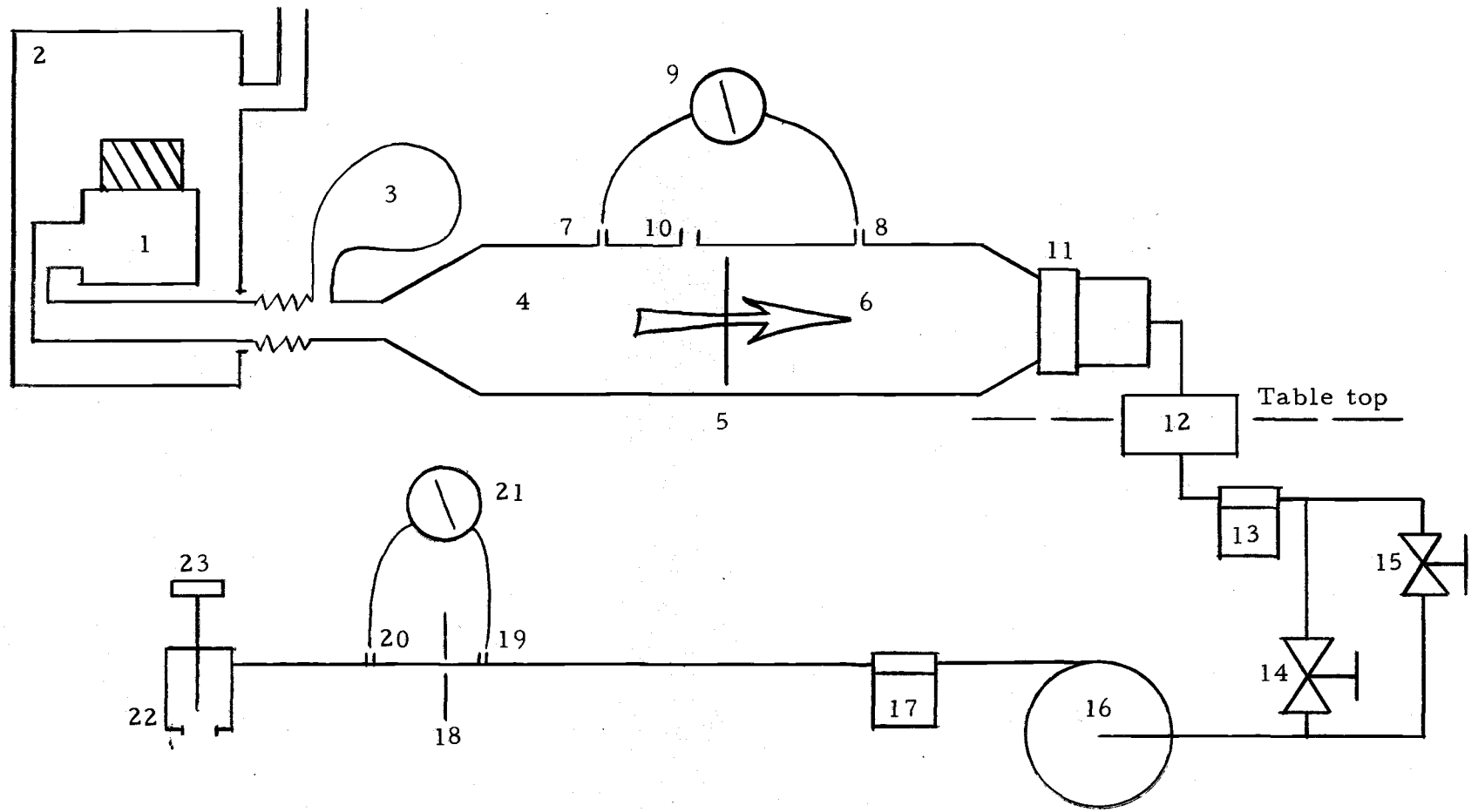

Figure 3. Schematic diagram of the filter test equipment. See Table 9 for description of components.

discussion of each component follows in Table 9. Figures 4 through 11 are photographs of the primary components.

The balance used for weighing filters, jars and dust was a fully enclosed Mettler type H15; accuracy = 0.05 mg, precision = 0.05 mg, readability = 0.1 mg. Maximum size of plane square object which will fit on the pan in the enclosure is approximately 6 inches. The laboratory oven used for evaporating methyl alcohol from the downstream flow tube wash jars was a Blue-M Stabil-Therm gravity oven with a temperature range of 0 - 290 C.

In addition, equipment was needed to determine the relationship between pressure drop and volume flow rate (or filter velocity) at much larger flow rates than those available from the filter test equipment shown in Figure 3. A Gelman plastic 1-inch paper filter holder was modified for this purpose. Effective filter area was 0.56 $in.^2$ (3.61 cm^2). The inlet was connected to a 2000 $Lbf/in.^2$ (10,000 cm Hg) compressed air cylinder and the outlet to a calibrated Gilmont flowmeter; range: 0 - 40,000 cm^3/min., accuracy = 2% of full scale. A Dwyer Magnehelic differential pressure gage was connected across the filter; range: 0 - 50 in. H_2O (0 - 9.35 cm Hg), accuracy = 2% of full scale. A schematic diagram of this apparatus is shown in Figure 12.

Table 9. Components of the filter test equipment. See Figure 3 for schematic diagram.

Component number	Description and purpose
1.	Particulate generator to provide sander dust to the filter test section. Modified Sears industrial 4-inch belt sander with dust pickup, Model 2267C. Sander belts are 3-M-ite: 4 x 24-inch, resin bond, 100 grit, open coat. A spring tension harness provides a variable predetermined force to the sanding block. Figure 4 shows the sander with wood block, spring tension harness, and ducting to pressure equilizer and flow tube inlet.
2.	Dust enclosure to prevent leakage dust from entering the testing room; connected to the building ventilation exhaust line. See Figure 5.
3.	Pressure equilizer to collect excess dust and provide a means of equilizing the upstream flow tube pressure to ambient. Fabric dust collector supplied with Sears belt sander, Model 2267C. See Figure 5.
4.	Upstream flow tube to provide air flow and sander dust uniformly to the filter test section, and to provide for direct observation of the filtering process during testing. Straight run is 0.125-inch wall x 6-inch O.D. x 24-inch long plexiglass tubing. Entrance cone was formed from 0.125-inch plexiglass sheet; approximately 2-inch inlet I.D. x 8.4-inch long. See Figures 5 through 8.
5.	Filter test section to provide support, seal and ease of access to test filters. Filter test area is 25-in.^{2}. Four springs provide a total closing force of 88 Lbf, distributed around the tube filter seal. A removable shoe is

Table 9. Continued.

Component number	Description and purpose
	provided for calibrating filter dust fall-off. See Figure 6 through 8.
6.	Downstream flow tube to provide exhaust from filter test section and entrance to Nuclepore section. Rotates to vertical (down) position for washing out the collected dust particles. Straight run is 0.125-inch wall x 6-inch O.D. x 24-inch long plexiglass tubing. Exit cone was formed from 0.125-inch plexiglass sheet; approximately 3.75-inch outlet O.C. x 7.5-inch long. See Figure 6, 7 and 9.
7.	Upstream pressure tap for filter test section to provide for measurement of Porex pressure drop. Located 12 inches ahead of filter test section. See Figures 6 through 8.
8.	Downstream pressure tap for filter test section. Located 12 inches behind filter test section. See Figure 6.
9.	Differential pressure gage to indicate Porex pressure drop. Dwyer Magnehelic gages; ranges: 0 - 2, 0 - 4, 0 - 10, in. H_2O. Accuracy is within 2% of full scale. See Figures 6, 7 and 9.
10.	Entry ports (two each) for hot wire anemometer probe to provide for calibration of flow rates and velocities. Plexiglass; located 4.5 inches ahead of filter test section. See Figures 7 and 8.
11.	Nuclepore section to provide support, seal and ease of access to Nuclepore filters. Machined from a 2-1/2-inch brass coupling to support 9-cm diameter filters.

Table 9. Continued.

Component number	Description and purpose
	Epoxy bonded to downstream flow tube. See Figures 6, 10 and 11.
12.	Filter to provide secondary protection from dust for the vacuum pump. Aluminum.
13.	Filter to provide primary protection from dust for the vacuum pump. Felt filter provided with the pump. See Figure 11.
14.	Valve to provide gross flow control. 3/8-inch (pipe) brass gate valve. See Figure 11.
15.	Valve to provide fine flow control. Whitey 1/4-inch (tubing) modified needle valve. See Figure 11.
16.	Vacuum pump to provide system flow. Gast: Oilless, carbon-vane type, 1/2 Hp, 1720 RPM, 7.2 cfm free flow; Model 0822-103-G271X.
17.	Silencer to provide quiet operation and to prevent carbon from entering flow meter orifice. Felt filter provided with pump. See Figure 11.
18.	Orifice to provide pressure drop for measuring system flow rate. Sharp-edge aluminum. Pipe I.D. is 0.875 inch, orifice I.D. is 0.414 inch. Figure 11 shows a portion of the upstream meter run.
19.	Upstream orifice pressure tap for measurement of orifice pressure drop to provide knowledge on system volumetric flow rate. Located 2.19 inches ahead of orifice.
20.	Downstream orifice pressure tap. Located 7 inches behind orifice.

Table 9. Continued.

Component number	Description and purpose
21.	Differential pressure gage to indicate orifice pressure drop, and therefore, system volumetric flow rate. Dwyer Magnehelic gages; ranges: 0 - 4 and 0 - 10 in. H_2O. Accuracy is within 2% of full scale.
22.	Orifice exhaust plenum to provide location for exhaust thermometer.
23.	Thermometer to measure exhaust temperature. Weston, stainless steel stem type; range: -40 to 120 F.

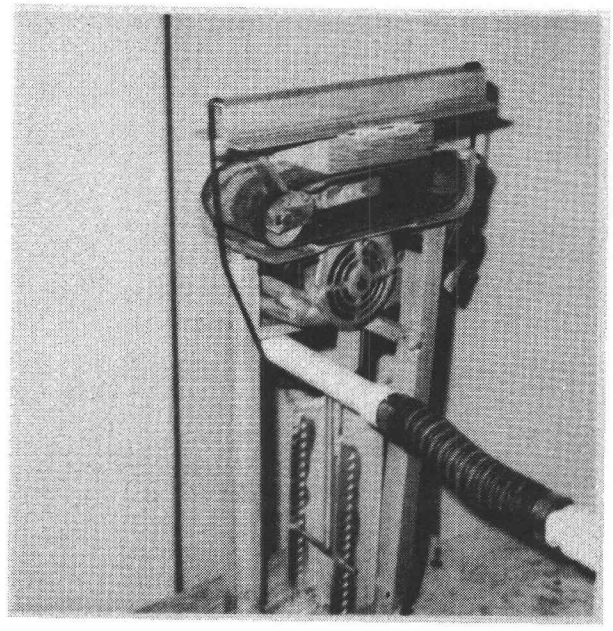

Figure 4. Sander dust generator.

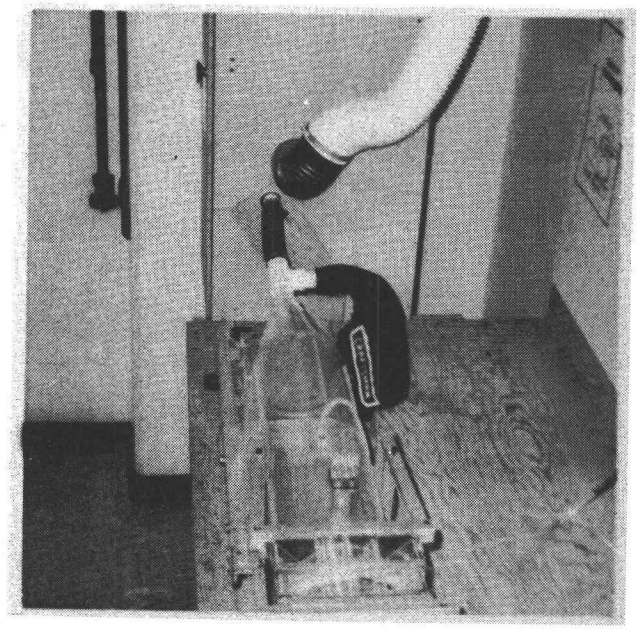

Figure 5. Dust enclosure, pressure equilizer and upstream flow tube.

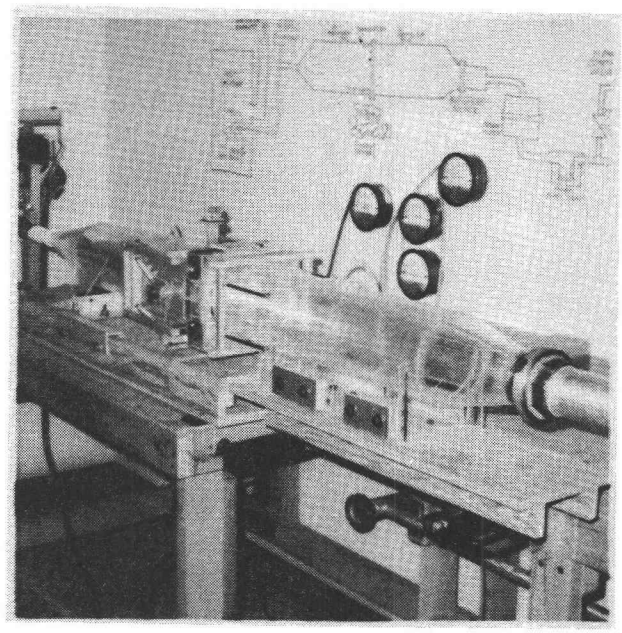

Figure 6. Filter test section with upstream and downstream flow tubes and Nuclepore holder.

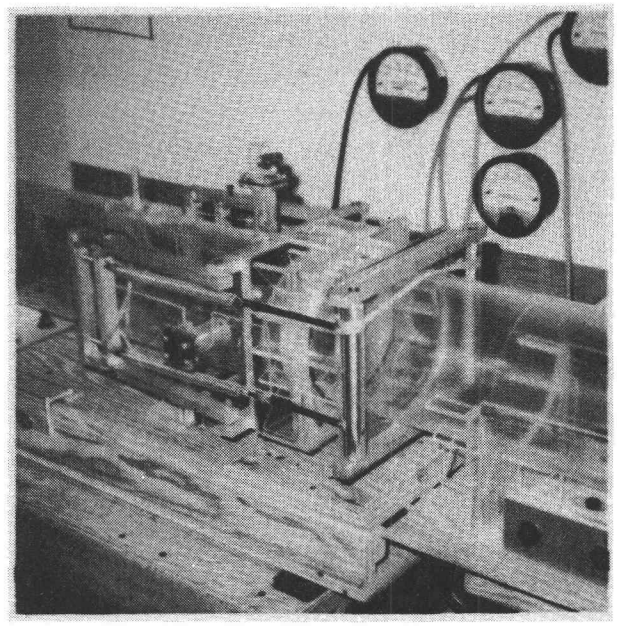

Figure 7. Filter test section close-up (closed).

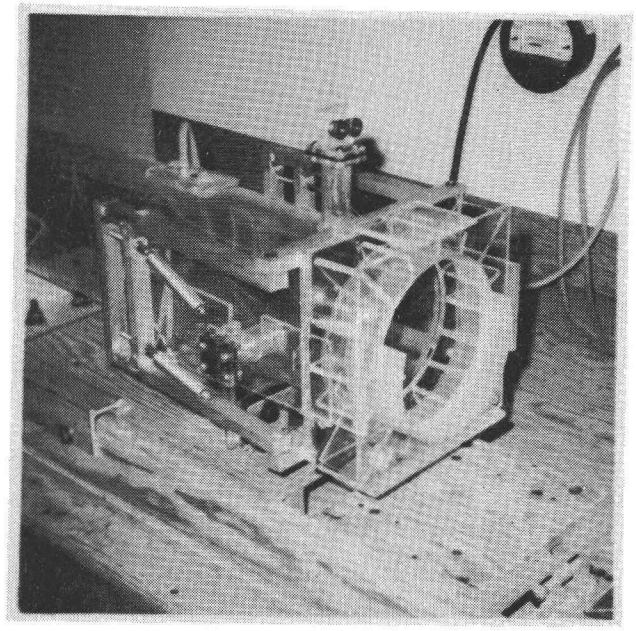

Figure 8. Upstream filter test section (open) with exposed dust fall-off shoe.

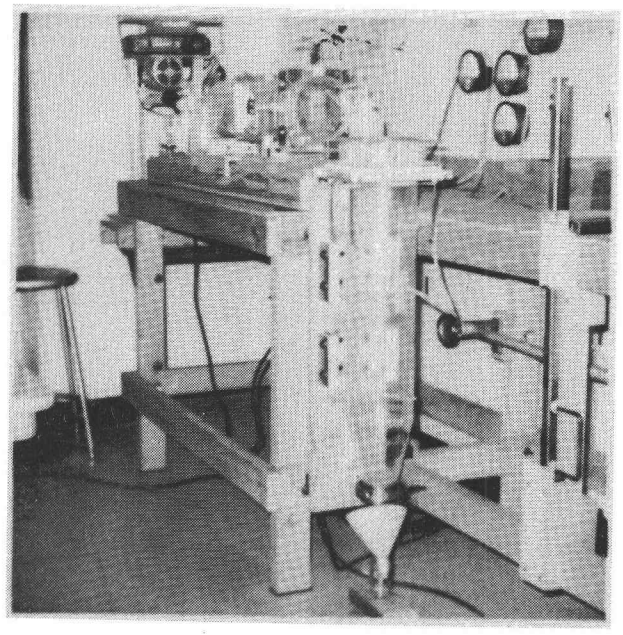

Figure 9. Downstream flow tube in down position.

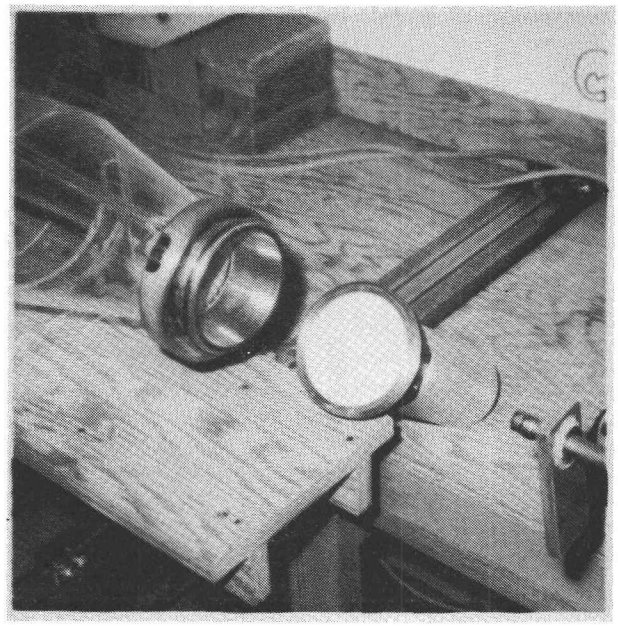

Figure 10. Nuclepore section (open).

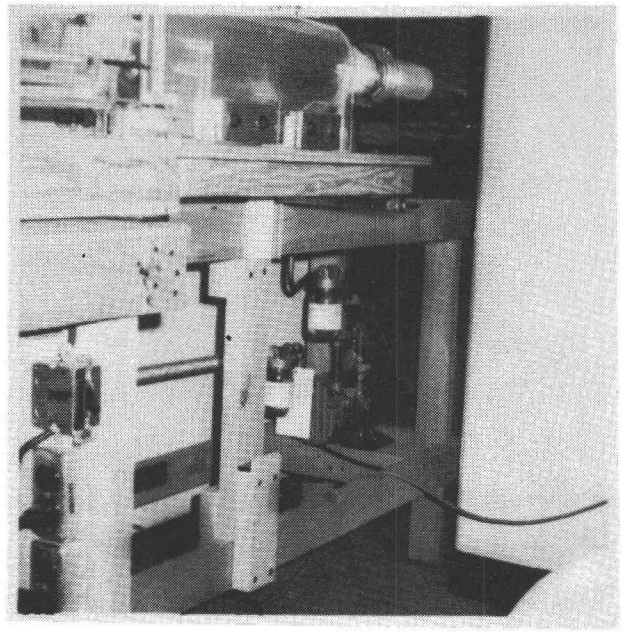

Figure 11. Vacuum pump and orifice flow tube.

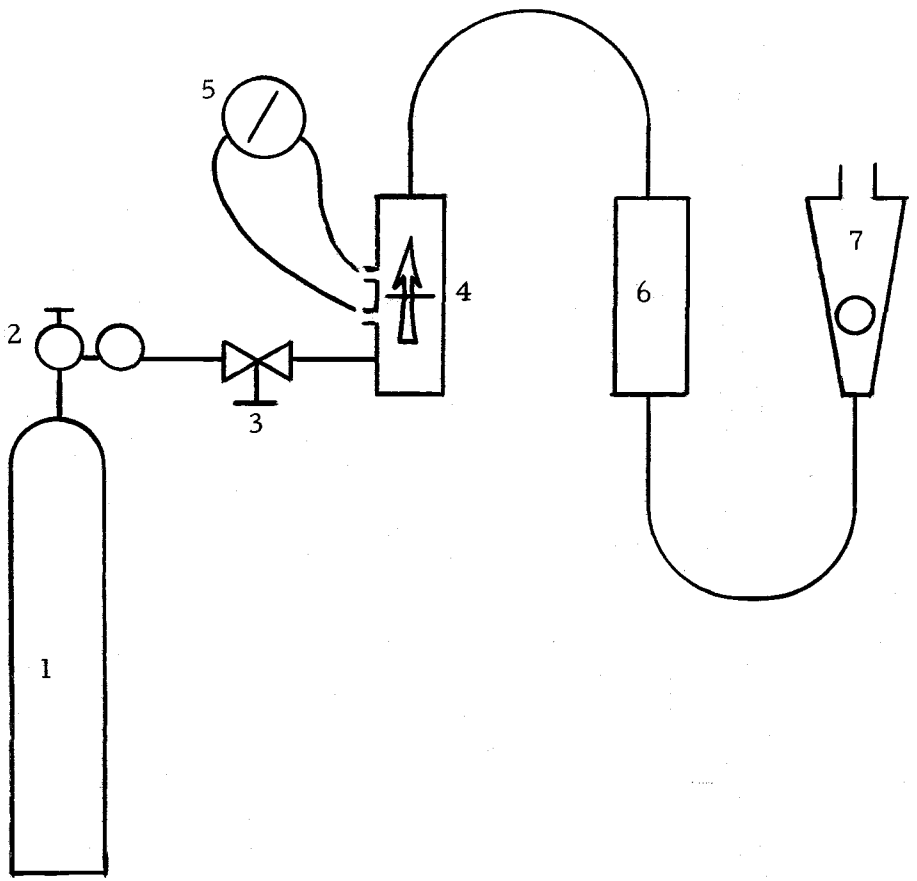

1. Air cylinder
2. Regulator
3. Needle valve
4. Filter section
5. Differential pressure gage
6. Mist eliminator
7. Flowmeter

Figure 12. Schematic diagram of the filter flow test apparatus.

Flow Calculations and System Calibrations

The orifice system was designed according to a procedure outlined in Handbook E-2 published by the American Meter Company (2). Flow calibration of the orifice was accomplished by a method involving the use of a saran bag with a known (calibrated) volume of 6.42 ft^3 [0.182 m^3]. After the bag was evacuated and connected to the orifice exhaust, the pump was turned on and the time for the bag to fill is recorded. The bag was considered full when a differential pressure gage connected between the bag and ambient indicated 2 in. H_2O [0.374 cm Hg]. For each calibration run, the following information was recorded.

1. Run number
2. Orifice pressure drop
3. Elapsed time to fill bag
4. Ambient pressure
5. Pressure drop between ambient and the downstream orifice tap
6. Orifice temperature
7. Bag temperature
8. Ambient temperature

The basic flow equation for a sharp-edged orifice is:

$$Q_m = C' [h_w p_f]^{1/2}$$

Where:

Q_m = Volumetric flow rate at desired conditions [ft^3/min]

h_w = Orifice pressure differential [in. H_2O]

p_f = Flowing pressure (absolute pressure at downstream orifice tap) [$Lbf/in.^2$]

$[h_w p_f]^{1/2}$ = Pressure extension

C' = "Constant"

$= F_b \times F_{pb} \times F_{tb} \times F_g \times F_{tf} \times F_r \times Y \times F_{pv} \times F_m$

Where:

F_b = Basic orifice factor (unknown)

F_{pb} = Pressure base factor = $14.73/P_b$

F_{tb} = Temperature base factor = $(460 + T_b)/520$

F_g = Specific gravity factor = 1

F_{tf} = Flowing temperature factor = $[520/(460 + T_f)]^{1/2}$

F_r = Reynolds number factor = $1 + [b/(h_w p_f)^{1/2}]$

F_{pv} = Supercompressibility factor = 1

F_m = Manometer factor = 1

Y = Expansion factor = 1

P_b = Base pressure (pressure at which Q_m is determined) [$Lbf/in.^2$]

T_b = Base temperature (temperature at which Q_m is determined) [F]

T_f = Flowing temperature (temperature at downstream orifice tap) [F]

b = Unknown constant [(in. H_2O x Lbf/in.^{2})$^{1/2}$]

Thus

$$C' = F_b \left[\frac{14.73}{p_b}\right]\left[\frac{460 + T_b}{520}\right]\left[\frac{520}{460 + T_f}\right]^{1/2}\left[1 + \frac{b}{(h_w p_f)^{1/2}}\right]$$

In general, base conditions may be selected arbitrarily at the values for desired flow conditions. This allows us to determine the flow rate at desired conditions rather than at existing actual conditions. However, for calibration purposes, the measured volume is at some actual condition of temperature and pressure. Therefore, in this case, T_b and p_b must refer to actual bag conditions if the actual bag volume is to be used.

In the present case, each data point was converted to represent the values which would have existed if the bag had been at standard conditions and the flowing conditions had been 14.73 Lbf/in.^{2} [76 cm Hg] and 110 F [43 C]. This was accomplished as follows.

Define a new "constant"

$$C = F_b \left[1 + \frac{b}{(h_w p_f)^{1/2}}\right]$$

So that

$$Q_m = C\left[\frac{14.73}{p_b}\right]\left[\frac{460 + T_b}{520}\right]\left[\frac{520}{460 + T_f}\right]^{1/2}[h_w p_f]^{1/2}$$

$$= C \cdot X \cdot Y \cdot Z \cdot [h_w p_f]^{1/2}$$

or

$$C = \frac{Q_m}{X \cdot Y \cdot Z \cdot [h_w p_f]^{1/2}}$$

The value of C was determined for each data point using actual values in the calculation. That is

Setting Q_m = Bag volume/time to fill

p_b = Actual bag pressure = barometric pressure

T_b = Actual bag temperature

T_f = Actual flowing temperature

h_w = Actual orifice differential pressure

p_f = Actual flowing pressure

Then, for each point, we see that

$$Q_b = C\left[\frac{520}{460 + T_f}\right]^{1/2}[h_w p_f]^{1/2}$$

Where Q_b is the volumetric flow rate at standard conditions. If we now set T_f = 110 F [43 C] in this equation for each data point, we will have standardized the data to represent the flow rate at standard

conditions for the specified flowing temperature. Designating this flow rate Q_b at T_f = 110 F [43 C] as Q_b', Q_b' was plotted against pressure extension.

Consideration of the equation above for Q_b' shows that

$$Q_b' = F_b \left[1 + \frac{b}{(h_w p_f)^{1/2}}\right] \left[\frac{520}{570}\right]^{1/2} [h_w p_f]^{1/2}$$

$$= \left[\frac{520}{570}\right]^{1/2} F_b\, b + \left[\frac{520}{570}\right]^{1/2} F_b [h_w p_f]^{1/2}$$

Thus, for constant values of F_b and b, Q_b' should be a linear function of pressure extension.

Observation of the plotted data showed this to be true for values of $Q_b' > 2$ standard ft^3/min [943 cm^3/sec]. Consequently, a least squares fit to the data was made, resulting in the values $F_b = 0.389$ and $b = -0.656$ with appropriate units to match those specified earlier.

Thus, our formal equation becomes (for $Q_b > 2$)

$$Q_b = \left[\frac{520}{460 + T_f}\right]^{1/2} [-0.255 + 0.389 (h_w p_f)^{1/2}]$$

In Figure 13, standard volumetric flow rate is plotted against $(h_w p_f)^{1/2}$, called pressure extension, over a range of values for T_f. To aid in the use of Figure 13, pressure extension is plotted

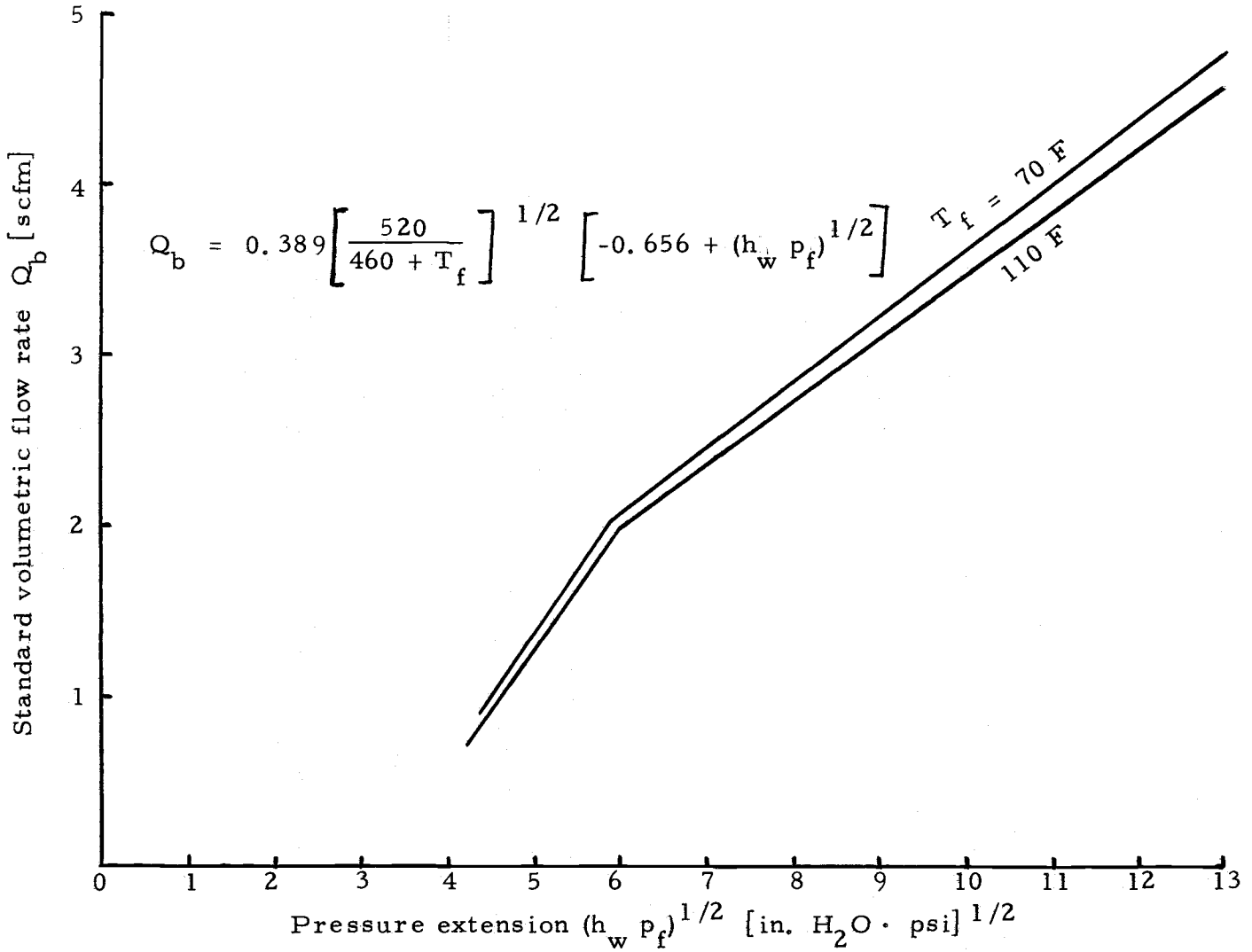

Figure 13. Flow system orifice calibration.

against orifice pressure drop over a range of values of p_f in Figure 14.

Next, it was necessary to know the true value of filter velocity at the filter test section over a range of values of temperature, T_o, and pressure, p_o, for known values of Q_b. Assuming a perfect gas, it is easy to show that

$$Q_b = Q_o \left[\frac{p_o}{p_b}\right] \left[\frac{T_b}{T_o}\right]$$

Where the subscript o designates values at the upstream filter surface, then, since $Q_o = A_o v$,

$$Q_b = A_o v \left[\frac{p_o}{p_b}\right] \left[\frac{T_b}{T_o}\right]$$

Where:

A_o = Effective filter surface area = 26 in.^{2} [167 cm^2]

v = Filter velocity

Figure 15 is a plot of standard volumetric flow rate as a function of filter velocity over ranges of temperature and pressure (at the upstream filter surface).

The procedure for using Figures 13 through 15 is as follows:

1. For a desired v enter Figure 15 and locate Q_b for anticipated values of T_o and p_o.

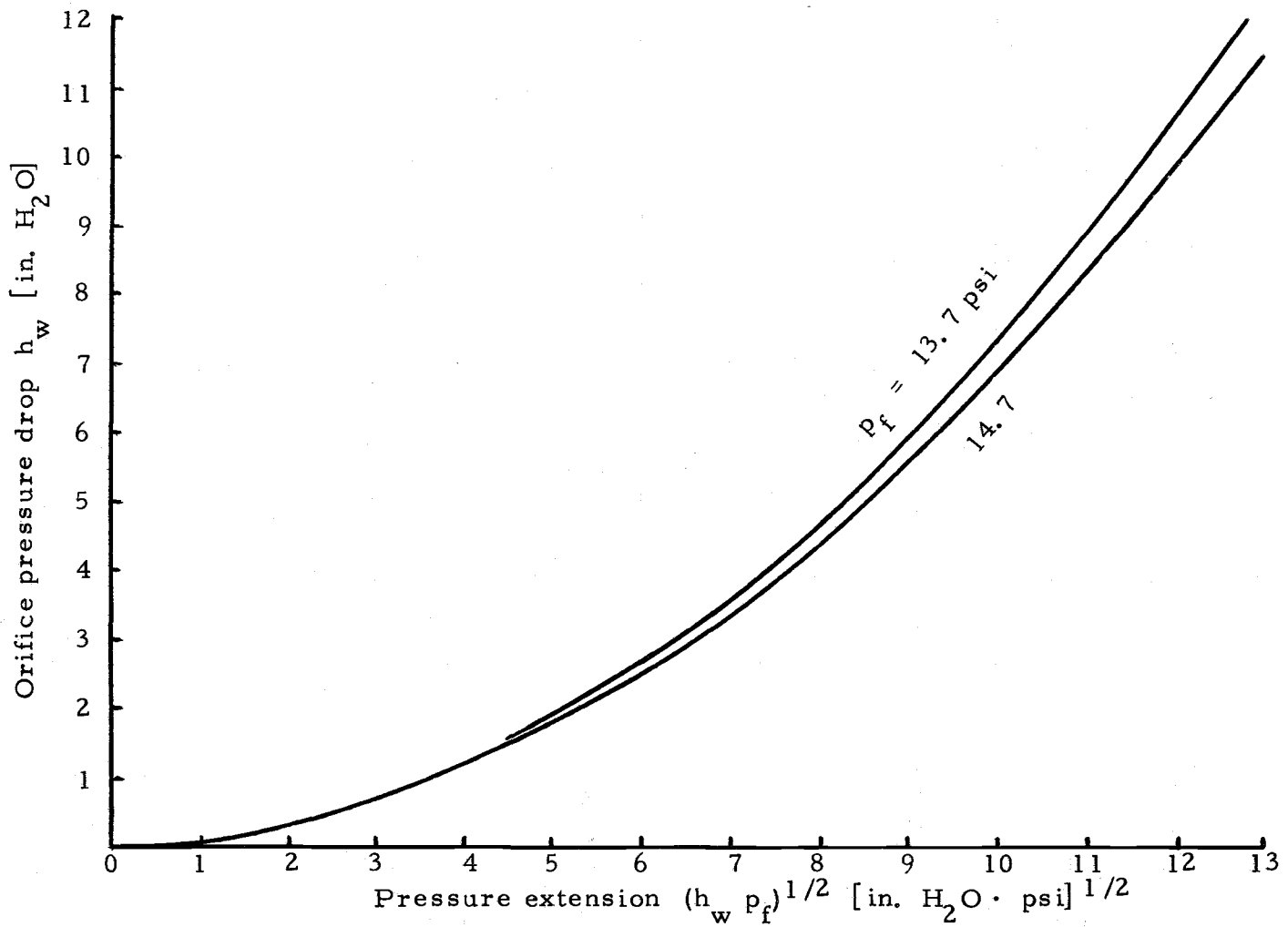

Figure 14. Pressure extension vs. orifice pressure drop.

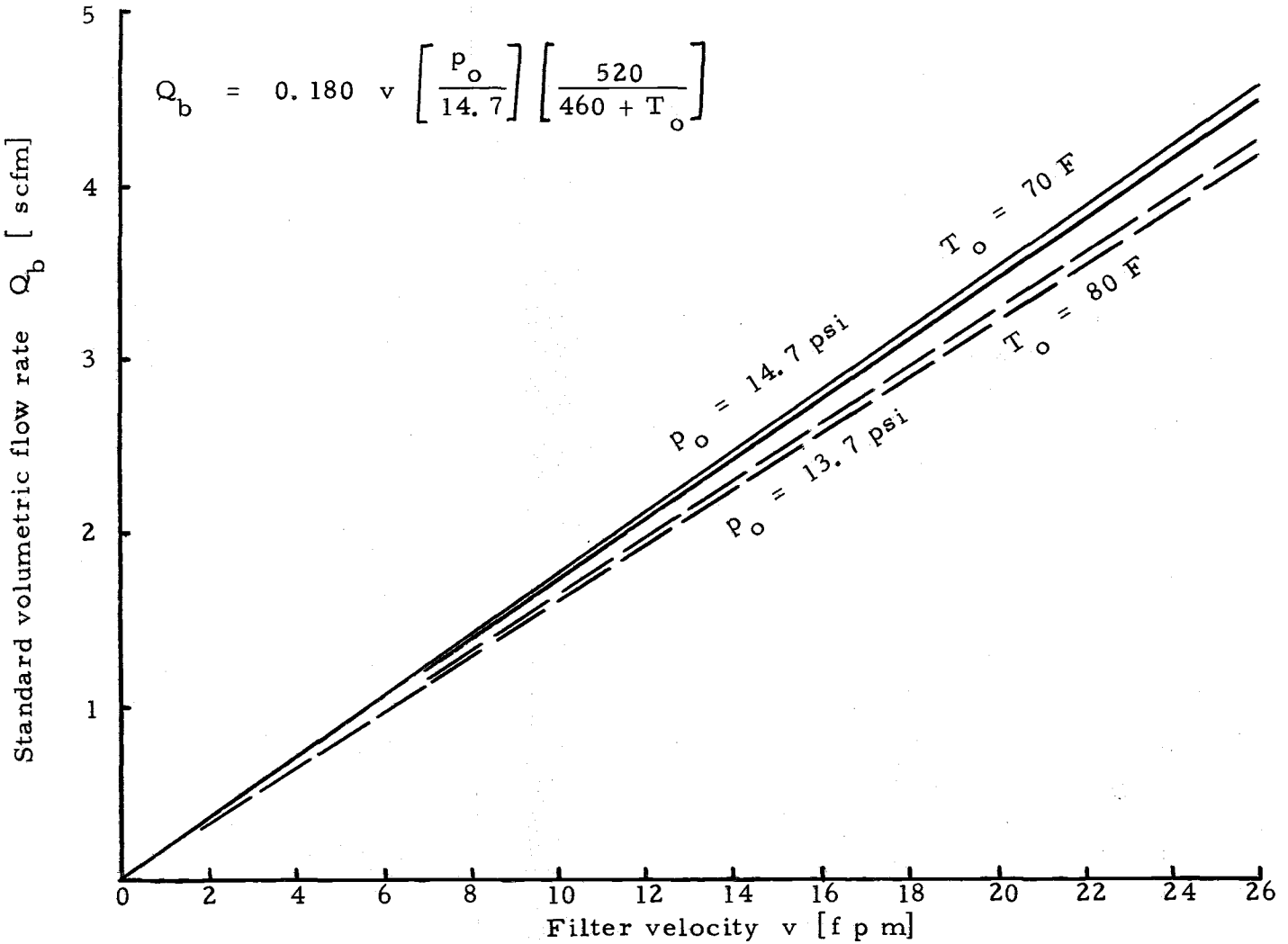

Figure 15. Filter velocity vs. standard volumetric flow rate.

2. Enter Figure 13 with Q_b and locate a value of pressure extension for an anticipated value of T_f.
3. Enter Figure 14 with the pressure extension and locate the required value of orifice pressure drop for an anticipated value of p_f.

The accuracies of the orifice calibration and the subsequent equations relating filter velocity to standard volumetric flow rate were checked using methods of hot wire anemometry. A Thermo-Systems hot wire anemometer was used with a 0.002-in. [0.005 cm] platinum hot film probe and an EAI Variplotter (x-y plotter). Vertical and horizontal traverse lines passing through the flow tube axis were used with a total of twelve sample points in three equal concentric areas according to a method described by the Los Angeles County Air Pollution Control District (25). Figures 7 and 8 show the probe ports. Each point was sampled for 25 seconds with the Variplotter pen traveling at a speed of 1 cm/sec. A planimeter was used to find the area under each plot and the average velocity determined by dividing this area by the sample time (25 sec). Finally, the total average was found by averaging the local averages.

Calibrations were made at 15 ft/min. [7.62 cm/sec] and 25 ft/min. [12.7 cm/sec] as indicated by orifice flow measurements. Although instantaneous point velocities varied greatly, the point averages were quite consistent. The velocities determined by

calibration were 15.3 ft/min. [7.77 cm/sec] and 25.6 ft/min. [13.0 cm/sec], respectively, which agree quite well with the orifice settings. The ratio of maximum instantaneous point velocity to average velocity was of the order 3 in both cases.

The flow system was leak checked by the following method.

1. With a system flow rate corresponding to the highest test flow rate, the static pressures at possible points of leakage were determined.
2. These points were individually isolated and connected to a small sealed vacuum pump. The pump flow rate was adjusted until the correct pressure was attained at the point.
3. The pump discharge was connected to a calibrated saran bag and the filling time was recorded so that the leakage flow rate was determined.
4. The leakage flow rate was determined as a percent of the system flow rate.

Note that in all cases the leakage must be into the system, since absolute system pressure must be below ambient at all points downstream from the filter test section. Results of the leak test are shown in Table 10.

Table 10. System leak test results.

Point	Leakage (%)	Remarks
Upstream Porex seal	0.0	No Δ p
Downstream Porex seal	1.5	Seal + filter end effect
Nuclepore seal	0.0	
Below Nuclepore	1.0	
Total	2.5	

During the tests, the Porex filters are held in a vertical position. Consequently, after a sufficient period of operation, the sander dust build up on the filter will be great enough that some will fall off onto the sides of the upstream flow tube during operation, during filter removal or both. Because the weight of dust which is prevented from passing through the filter is determined in this study by weighing the dust collected on the Porex filter, it is essential that the test period be sufficiently short to preclude fall-off from occurring.

The removable shoe shown in Figure 8 was used to calibrate the system to determine the maximum allowable buildup of dust on the Porex filter surface. In addition to the shoe, a 2-inch extension, placed between the upstream flow tube and the Porex filter, was required. Dust weights collected on the shoe, with and without the extension in place, were determined. It must be remembered that

some dust will fall on the shoe in every case due to dust fall-out from the moving particulate stream, but is not important because it does not first reach the Porex filter. Results of these calibration tests show that filter dust fall-off is not serious for collected masses up to 0.06 to 0.08 gm, and that the collected mass should never exceed 0.1 gm. Consequently, for the formal testing of the Porex filters, it was decided to attempt to achieve a total collected dust mass on each filter of from 0.05 to 0.07 gm.

Many unsuccessful attempts were made to obtain an accurate calibration curve for the dust generator in terms of mass loading as a function of block harness spring position and filter velocity. Unfortunately, the values were not consistent, primarily due to clogging of the sander and to sander belt wear, and the first generator was substantially redesigned because of this problem. Although the variability was never completely eliminated, choice of the proper sander belt proved to be a major improvement. 3-M-ite aluminum oxide belts designated as 100 grit, resin bond, open coat proved to be the most successful. Grit sizes smaller than 100 (larger "sand" particles) tended to remove dust particles which were too large and clogging of the sander increased. Open coat was an improvement over closed coat for the same reason. Aluminum oxide belt particles and resin bonding reduced belt wear rate. New belts were installed every 8 to 10 runs. In addition to using

improved belt design, satisfactory sander operation also required cleaning the dust pickup system between each run. This was accomplished by connecting a vacuum cleaner to the dust pickup system outlet and working out any plugged material with a piece of wire which was bent to fit into the inlet.

However, in spite of these precautions, accurate calibration was not accomplished. That is, for a given set of conditions, dust loading varied from test to test. Consequently, the block spring tension was set not only by considering the desired conditions, but also by observing the results of the previous test with respect to what had been desired. This technique worked reasonably well and was finally adopted as the best available method.

System Operating Procedure

The basic simplified steps required to test a single Porex filter at certain specified conditions of filter velocity and mass loading are as follows:

1. Tare Porex, Nuclepore and wash jar.
2. Install Porex and Nuclepore.
3. Set sander and flow conditions.
4. Turn on sander and flow system.
5. Observe dust buildup.
6. Turn off flow system and sander.

7. Record elapsed time.
8. Remove Porex and weigh.
9. Remove Nuclepore and weigh.
10. Lower downstream flow tube and rinse with methyl alcohol into wash jar.
11. Evaporate methyl alcohol.
12. Weigh wash jar.

Penetration weight is determined as the sum of Nuclepore net weight and jar net weight. Collected (or removed) dust is determined as the Porex net weight. Total dust reaching the Porex filter is the sum of penetration weight and removed dust, and the Porex efficiency is therefore

$$\eta = 1 - \frac{(\text{Nuc. net} + \text{jar net})}{\text{Porex net} + \text{Nuc. net} + \text{jar net}}$$

Note however that this simplified procedure does not include the necessity for statistical control.

The complete filter test procedure followed during each test run is considerably more complex and is outlined in Table 11.

Data Recording Procedure

The procedure for operating the test equipment has been outlined in Table 11, and within that procedure several of the steps

Table 11. Filtration test procedure.

1. Turn enclosure ventilation ON.
2. Record "Run" number.
3. Record "Date" and "Time."
4. Record experimental order code.
5. Record desired "Filter Velocity."
6. Record desired "Mass Loading."
7. Record "Ambient Temp."
8. Record "Ambient Pres."
9. Record "Rel. Humidity."
10. Determine and record desired "Orifice Setting."
11. Determine and record desired "Spring Position."
12. Record desired "Mass Collected."
13. Determine and record desired "Mass Flow Rate."
14. Determine and record desired "Length of Run."
15. Record desired addition to run length.
16. Record "Porex #."
17. Record "Jar #."
18. Raise downstream tube.
19. Remove Nuclepore ring horseshoe.
20. Tare jar and record as "Jar-Tare."
21. Tare control jar and record as "CJar-Tare."
22. Tare Nuclepore and record as "Nuclepore-Tare."
23. Insert Nuclepore into holder and secure ring.
24. Connect tubing to Nuclepore holder.
25. Tare Porex and record as "Porex-Tare."
26. Remove downstream tube cover.
27. Install Porex and secure spring locks.
28. Connect filter pressure hoses to appropriate gage.
29. Turn pump ON.

Table 11. Continued.

30. Adjust flow control valves to proper orifice setting.
31. Turn pump OFF.
32. Open enclosure door.
33. Check sander connections.
34. Check block for wear and position.
35. Set proper spring position.
36. Install dust bag.
37. Connect sander exhaust to tube inlet.
38. Zero stop watch.
39. Close enclosure door.
40. Turn sander ON.
41. Turn pump ON.
42. Turn stop watch ON.
43. Record "Porex Δp" as required.
44. Record "Up-Tap Δp."
45. Adjust sander belt as required.
46. Turn pump OFF.
47. Turn stop watch OFF.
48. Turn sander OFF.
49. Open enclosure door.
50. Record "Orifice Temp."
51. Record "Length of Run."
52. Disconnect sander exhaust from tube inlet.
53. Remove dust bag.
54. Disconnect sander block spring harness.
55. Close enclosure door.
56. Release filter spring locks.
57. Slide upstream tube full toward sander.
58. Remove Porex.

Table 11. Continued.

59. Install downstream tube cover.
60. Weigh filter and record as "Porex - Final."
61. Disconnect tubing from Nuclepore holder.
62. Unscrew Nuclepore ring and remove holder.
63. Remove Nuclepore from holder.
64. Weigh Nuclepore and record as "Nuclepore - Final."
65. Lower downstream tube.
66. Insert Nuclepore ring horseshoe.
67. Vacuum clean upstream tube.
68. Place jar with funnel beneath downstream tube.
69. Remove downstream tube cover.
70. Rinse downstream tube thoroughly into jar.
71. Install downstream tube cover and allow tube to dry.
72. Rinse funnel into jar.
73. Screw lid onto jar.
74. Remove downstream tube cover.
75. Rinse downstream tube thoroughly into control jar.
76. Install downstream tube cover and allow tube to dry.
77. Rinse funnel into control jar.
78. Screw lid onto control jar.
79. Connect vacuum cleaner to sander exhaust.
80. Open enclosure door.
81. Remove sander connection.
82. Remove block and spring harness.
83. Vacuum clean sander blower inlet.
84. Vacuum clean sander dust inlet while removing clogged dust with wire.
85. Install sander connection
86. Install block and spring harness.

Table 11. Continued.

87.	Close enclosure door.
88.	Turn lab oven ON. Set to 60°C.
89.	Remove jar lid and control jar lid.
90.	Place jar and control jar in oven overnight.
91.	Remove jar and control jar from oven.
92.	Turn oven OFF.
93.	Screw on lids (not tight).
94.	Let equilibrate.
95.	Remove jar lid and control jar lid.
96.	Weigh jar and record as "Jar - Final."
97.	Weigh control jar and record as "CJar - Final."

End of Test Run

require the recording of test data. To simplify this data collection, a data sheet was devised, and each test run required a separate data sheet. A sample data sheet with actual raw data from Test Run Number 30 is shown in Figure 16. The data which required calculation, such as Porex penetration, are included. Nuclepore (gm), as shown on the data sheet, is the mass of dust reaching the Nuclepore filter, and Nuclepore (gm/gm) is the fraction of dust reaching the Porex filter which is collected on the Nuclepore. Porex Penetration (%) is the percent of dust mass reaching the Porex filter which passes through (penetrates) the filter. Efficiency (as a fraction) is by definition equal to 1 - penetration (as a fraction). Total penetration is estimated from the following equation.

$$\phi \simeq \frac{\text{Nuclepore Net} + [\text{Jar Net} - \text{CJar Net}]}{\text{Porex Net}}$$

Experimental Design

A 2 x 3 x 3 factorial experiment with three complete replications was used with pore size, filter velocity and mass loading as the factors. There were two pore sizes: d_1 = 19 μm and d_2 = 32 μm; three filter velocities: v_1 = 15 ft/min [7.62 cm/sec], v_2 = 20 ft/min [10.2 cm/sec] and v_3 = 25 ft/min [12.7 cm/sec]; and three mass loadings: m_1 = 0.005 gm/ft^3 [0.175 μg/cm^2], m_2 = 0.01 gm/ft^3 [0.353 μg/cm^3] and m_3 = 0.015 gm/ft^3 [0.53 μg/cm^3]. However,

Run: 30 | Filter Velocity: 25 fpm

Date: 1-13-73 | Orifice Setting: 10.2 in. H_2O

Time: 1730 | Mass Loading: .015 gm/scf

Pore Size: A (19) µm | Spring Position: S2

Ambient Temp: 73 F | Mass Collected: .05 gm

Ambient Pres: 14.7 psi | Mass Flow Rate: .04 gm/min

Rel Humdiity: / % | Length of Run: 1.25 +4.8 sec min

Up-Tap Δp: 1.4 in. H_2O | Porex #: A 49

Orifice Temp: 80 F | Jar #: 5 CJar #: 15

Time	Porex Δp		Porex	Nuclepore	Jar	CJar
0.00	2.62	Final:	10.8116	.06482	115.83092	117.57162 gm
0.25	2.69	Tare:	10.7459	.06470	115.82592	117.56702 gm
0.50	2.77	Net:	.0657	.00012	.00500	.00460 gm
0.75	2.82	Nuclepore		.00012 gm		.00183 gm/gm
1.00	2.87	(Jar - CJar)		.00040 gm		.00609 gm/gm
1.25		Nuc. +(Jar - CJar)		.00052 gm		.00791 gm/gm
1.50		Porex Penetration		.791 %		
2.00		Length of Run:		1.0 min		
2.50		Mass Loading:		.0149 gm/scf		
3.00		Volume Flow Rate:		4.42 scfm		
(min)	(in. H_2O)	Filter Velocity:		25.3 fpm		

Figure 16. Sample filtration data sheet.

because it was not possible to specify the exact value of mass loading before each run, a range of values was used with the above values considered as attempted or desired values. There were a total of $2 \times 3 \times 3 \times 3 = 54$ individual test runs.

IV. RESULTS

Data

A sample data sheet giving raw data for run number 30 was shown in Figure 16. Reduced efficiency data associated with all 54 test runs of this study are given in Table 12. Note that the data are not presented in the random order of the individual tests, but rather are given relative to their experimental order number, where the first digit represents pore diameter, the second filter velocity, the third mass loading and the fourth replicate. For example, the experimental order number 2312 represents the particular test run involving Porex pore diameter d_2 = 32 μm, filter velocity v_3 = 25 ft/min [12.7 cm/sec], mass loading m_1 = 0.005 gm/ft^3 [0.176 μg/cm^3] and the second replicate.

Within Table 12 the following nomenclature is used.

EON = Experimental order number

TRN = Test run number

d = Porex average pore size (μm)

v = Actual filter velocity (ft/min)

m = Actual mass loading (gm/ft^3)

N_I = Inertial impaction parameter = $\frac{\rho_p D_p^2 v_o}{9 \mu d P}$

where ρ_p = 0.625 gm/cm^3

D_p = 8.7 μm

Table 12. Reduced filtration data.

EON	TRN	d(μm)	v(fpm)	m(gm/scf)	N_I	Nuc	Tube	Tot
1111	49	19	15.0	0.0034	2.85	0.00225	0.00225	0.00451
2112	56	32	15.1	0.0042	1.70	0.00745	0.00158	0.00903
1213	50	19	19.7	0.0035	3.74	0.00556	0.01204	0.01760
2212	51	32	19.9	0.0048	2.24	0.00402	0.02334	0.02736
1311	14	19	25.3	0.0081	4.80	0.00034	-0.00631	-0.00597
2313	59	32	25.2	0.0034	2.84	0.00929	-0.00022	0.00907
1121	47	19	15.1	0.0067	2.87	0.00649	0.00000	0.00649
2122	5	32	15.1	0.0059	1.70	0.00300	0.01178	0.01478
1222	26	19	19.9	0.0093	3.78	0.00031	0.00417	0.00448
2221	10	32	19.9	0.0073	2.24	0.00515	-0.00246	0.00268
1323	45	19	25.3	0.0093	4.80	0.01008	0.00602	0.01610
2323	36	32	25.3	0.0084	2.85	0.00335	-0.00872	-0.00538
1133	23	19	15.2	0.0122	2.88	0.00018	-0.00317	-0.00299
2131	9	32	15.1	0.0090	1.70	0.00566	-0.01279	-0.00713
1232	12	19	19.9	0.0119	3.78	0.00470	-0.00663	-0.00193
2232	8	32	19.9	0.0118	2.24	0.00450	0.00413	0.00863
1331	29	19	25.3	0.0115	4.80	0.00032	0.00378	0.00409
2333	2	32	25.3	0.0125	2.85	0.00670	0.01286	0.01956
1113	16	19	15.1	0.0043	2.87	0.00039	0.01381	0.0142
2111	7	32	15.1	0.0046	1.70	0.00548	-0.00027	0.00521
1212	17	19	19.8	0.0038	3.76	0.00250	-0.00135	0.00115
2211	52	32	19.9	0.0048	2.24	0.00476	0.03214	0.03690
1312	43	19	25.3	0.0091	4.80	0.00199	-0.00557	-0.00358
2312	4	32	25.2	0.0045	2.84	0.00472	0.00635	0.01107
1122	48	19	15.1	0.0069	2.87	0.00155	0.00222	0.00377
2121	55	32	15.1	0.0059	1.70	0.00474	-0.00388	0.00086
1223	46	19	19.9	0.0101	3.78	0.00293	0.01645	0.01938

Table 12. Continued.

EON	TRN	d(μm)	v(fpm)	m(gm/scf)	N_I	Nuc	Tube	Tot
2222	60	32	19.9	0.0095	2.24	0.00162	0.00061	0.00222
1321	41	19	25.3	0.0095	4.80	0.00285	0.00455	0.00740
2322	58	32	25.4	0.0095	2.86	0.00549	0.01420	0.01969
1131	24	19	15.2	0.0170	2.88	0.00222	0.01489	0.01711
2132	31	32	15.2	0.0246	1.71	0.00135	0.00834	0.00969
1231	13	19	19.9	0.0126	3.78	0.00228	0.00379	0.00607
2231	37	32	19.9	0.0120	2.24	0.00271	0.00048	0.00319
1333	11	19	25.4	0.0141	4.82	0.00231	0.00501	0.00732
2331	39	32	25.3	0.0151	2.85	0.00450	0.00150	0.00601
1112	27	19	15.1	0.0058	2.87	0.00019	0.01907	0.01926
2113	40	32	15.1	0.0057	1.70	0.00336	0.00419	0.00755
1211	42	19	19.9	0.0059	3.78	0.00262	-0.00361	-0.00099
2213	1	32	19.9	0.0055	2.24	0.00583	0.00958	0.01540
1313	15	19	25.3	0.0092	4.80	0.00236	-0.01827	-0.01591
2311	57	32	25.4	0.0071	2.86	0.00638	0.00319	0.00957
1123	20	19	15.1	0.0087	2.87	0.00200	-0.00424	-0.00224
2123	35	32	15.1	0.0089	1.70	0.00327	0.00640	0.00967
1221	28	19	19.9	0.0104	3.78	0.00092	0.02514	0.02606
2223	34	32	19.9	0.0103	2.24	0.00377	0.01020	0.01437
1322	25	19	25.4	0.0107	4.82	0.00643	0.00587	0.01230
2321	3	32	25.3	0.0101	2.85	0.00358	-0.00323	0.00036
1132	19	19	15.1	0.0181	2.87	0.00154	0.00237	0.00391
2133	54	32	15.1	0.0247	1.70	0.00042	-0.01107	-0.01066
1233	21	19	20.0	0.0253	3.80	0.00180	0.01218	0.01400
2233	32	32	19.9	0.0149	2.24	0.00438	0.00257	0.00694
1332	30	19	25.3	0.0149	4.80	0.00183	0.00609	0.00791
2332	33	32	25.3	0.0163	2.85	0.00145	-0.00367	-0.00222

v_o = v (above)

μ = 185 $(10)^{-6}$ gm/sec-cm

d = d (above)

P = 0.40

Nuc = Fraction of dust mass reaching the Porex filter which is collected by the Nuclepore filter.

Tube = Fraction of dust mass reaching the Porex filter which is collected in the tube washings.

Tot = Total fraction of dust mass reaching the Porex filter passing through the Porex filter = Nuc + Tube = Penetration (ϕ).

Note that test run numbers 6, 18, 22, 38, 44 and 53 are missing from the data. This is due to the inclusion of block controls in the original test scheme. However, it soon became apparent that controls would be required for every run. Consequently, controls were recorded on the data sheets for each run and the controls originally scheduled were omitted. Figure 17 presents the Nuc and Tot data for filters "A" and "C" as functions of N_I. Recall that for filter "A" the average pore diameter is 19 μm and for filter "C" it is 32 μm. The dashed lines connect the average Nuc values while the solid lines connect the average Tot values.

There are two important observations regarding the data of Table 12 which should be made here. Note the large variations in the data under the Tube column, plus observe that certain of the Tube and Tot data are negative. Of course, it is not physically possible to have

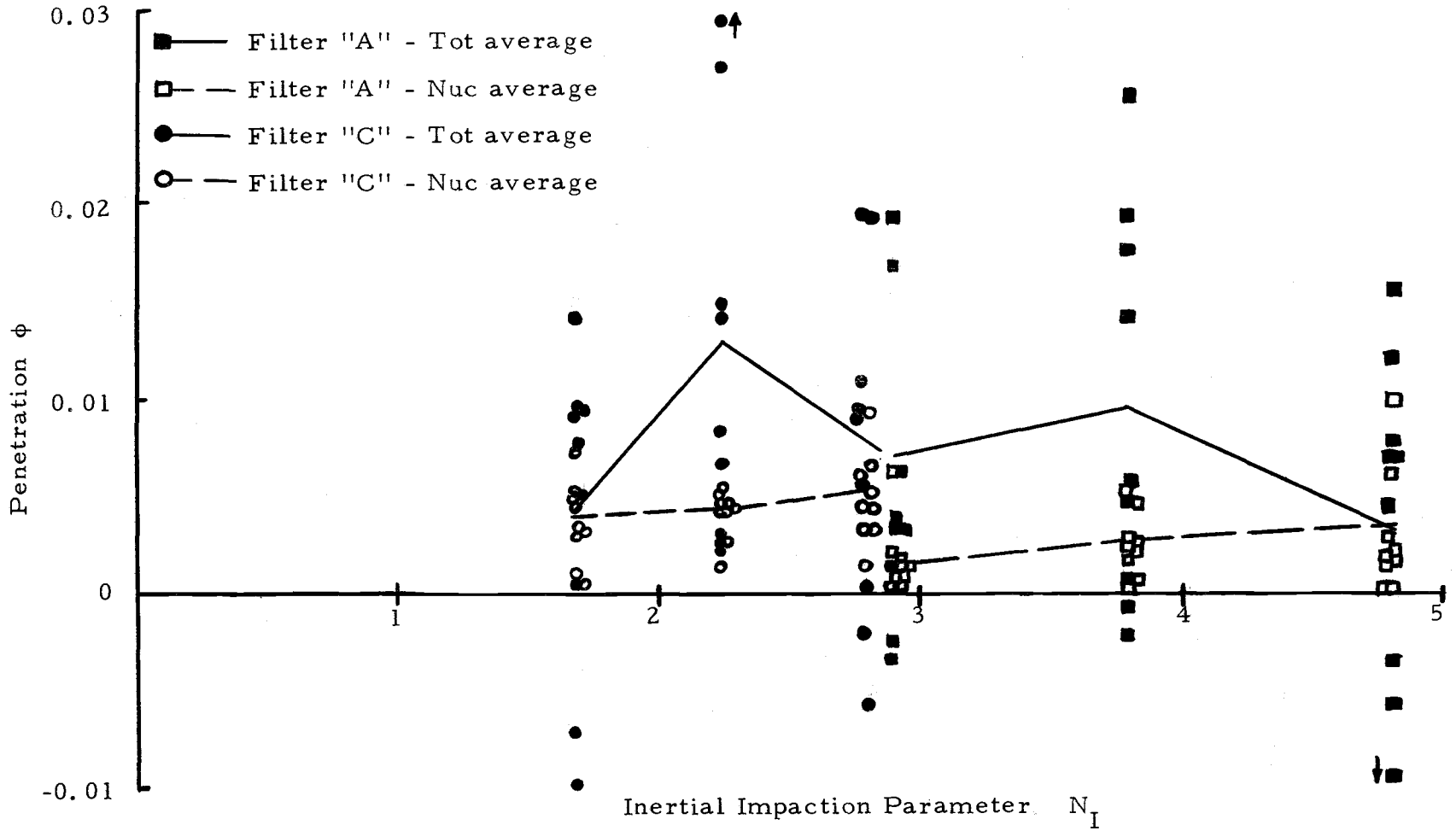

Figure 17. Penetration data vs. inertial impaction parameter.

a negative value of penetration. These phenomena will be considered later in this report under Interpretation of Results and Discussion of Errors.

Results of the pressure drop tests in the range of filter velocity used in the efficiency tests are shown in Figure 18. Differential pressure is plotted vs. filter velocity for the two filter sizes investigated. Roughly 150 data points were examined for each of the two groups. Only a representative sample of the data points is plotted.

Graphic Results

To aid in evaluation and verification of the data, two of the test filters were set in resin and cross-sectioned for microscopic analysis. Figures 19 and 20 show respective cross-sections of filter A-29 ($v = 25$ ft/min and $m = 0.015$ gm/ft^3) and filter C-154 ($v = 15$ ft/min and $m = 0.005$ gm/ft^3). Flow direction was from left to right and for reference the cover glass (on left edge of figures) is approximately 30 μm thick. In addition, electron micrographs were taken of the Nuclepore filter associated with filter C-154 in Figure 20. Figure 21 shows two of the micrographs. For reference, the pores are approximately 3 μm in diameter.

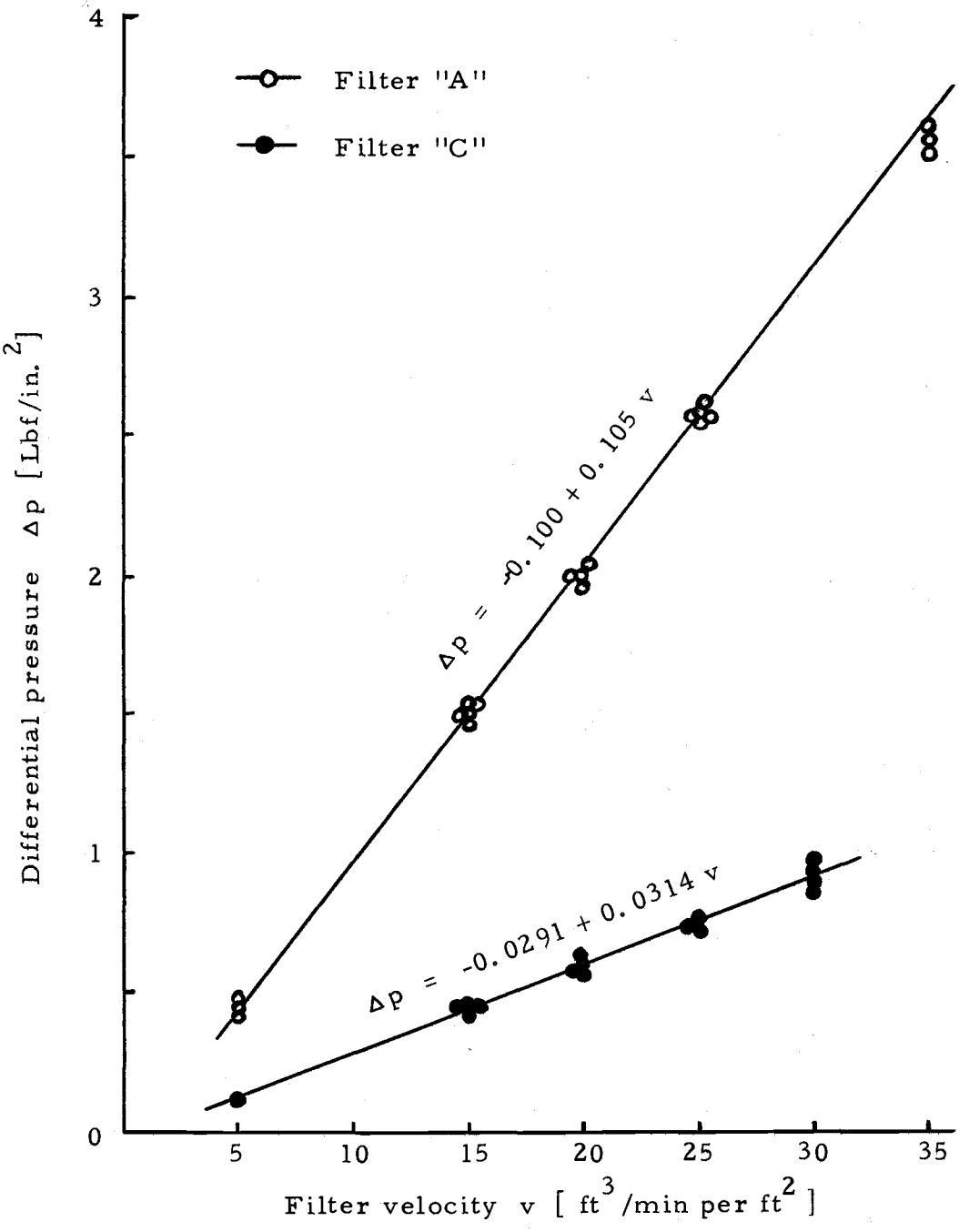

Figure 18. Pressure drop data.

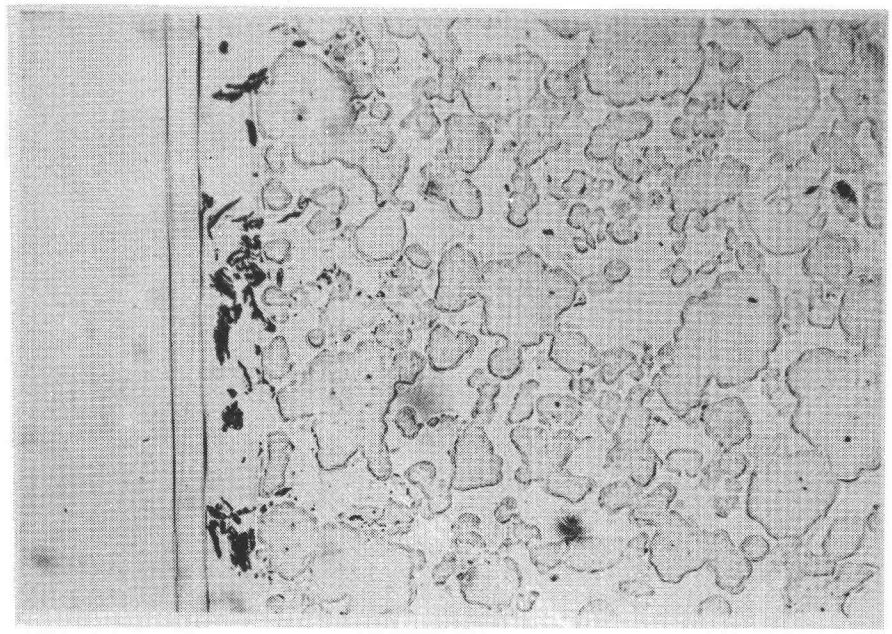

Figure 19. Filter A cross-section (cover glass is 30 μm thick).

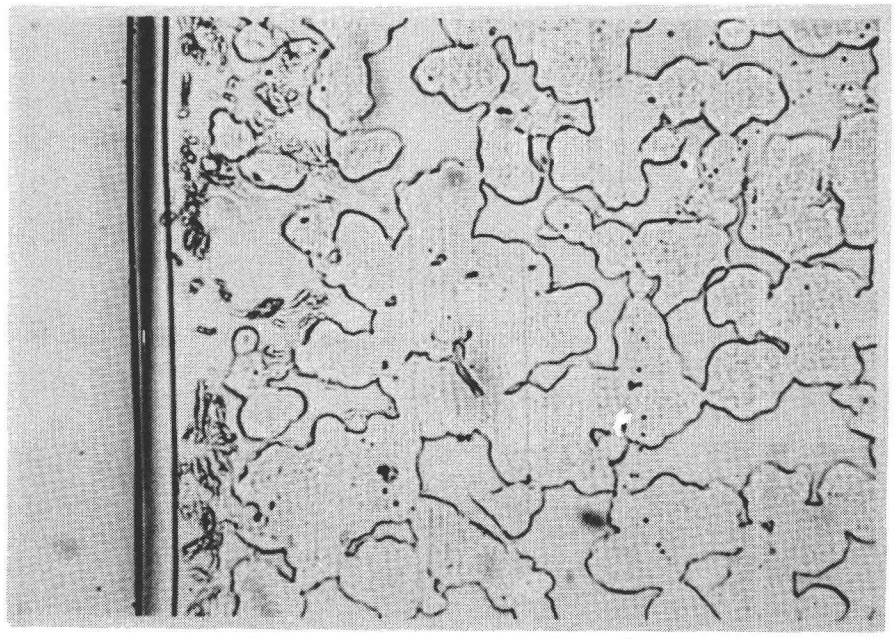

Figure 20. Filter C cross-section (cover glass is 30 μm thick).

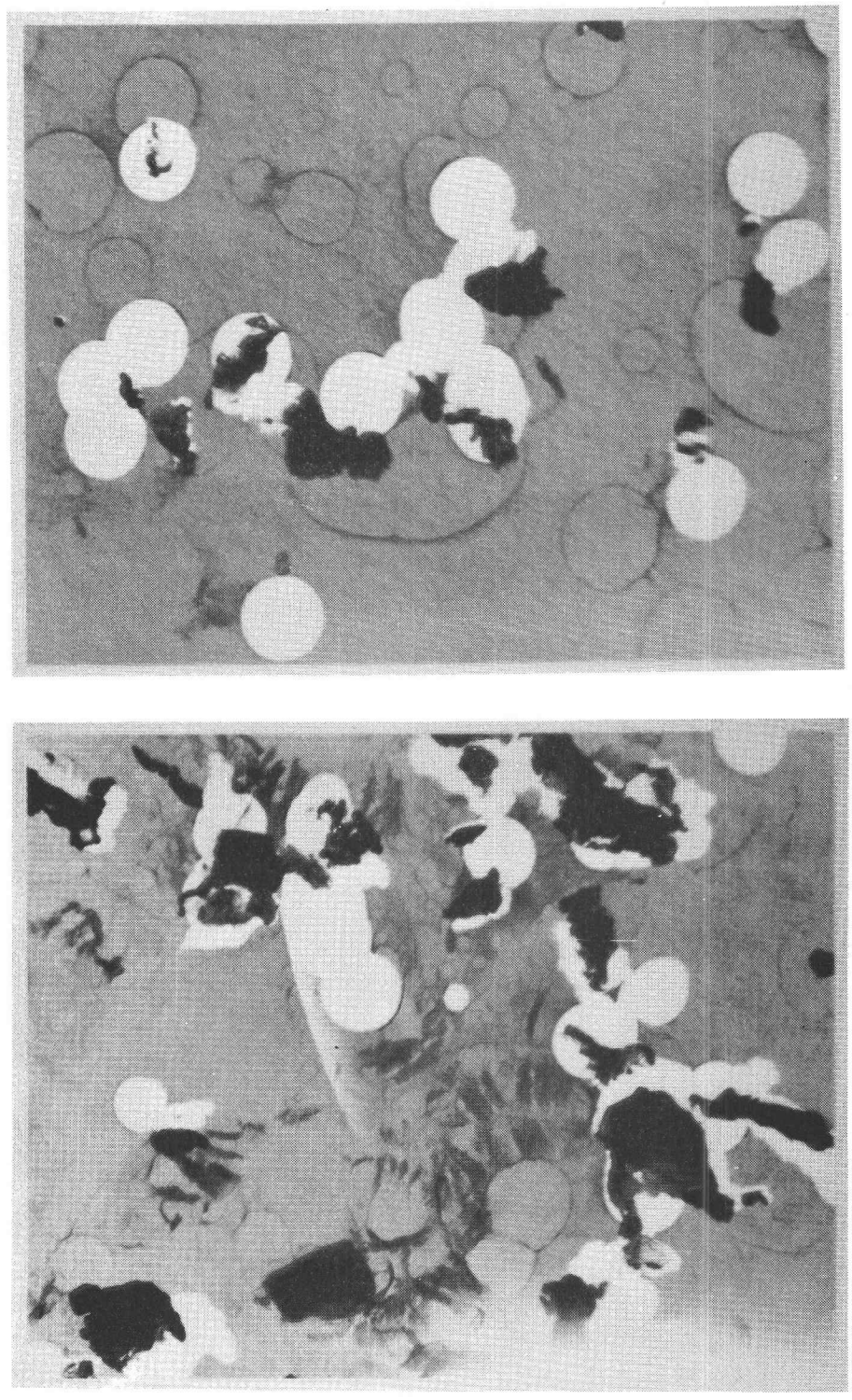

Figure 21. Nuclepore electron micrographs (pores are 3 μm diameter).

Statistical Analysis

The basic statistical analyses used are available on the Oregon State University OS3 computer as routine programs and are listed in the OSU Statistical Analysis Program Library. The two programs used were *NANOVA for n-factor analysis of variance, and *SIMLIN for simple linear regression. These terms are defined and the analyses described in most good books dealing with statistical inference. See, for example, Volk (46).

As pointed out above, the variations in the Tube values were quite large, as were those in the Tot values. Consequently, analyses were performed on data for Nuc and Tube, as well as Tot (our primary interest), to aid in the evaluation. Results of *NANOVA for the three terms are given in Tables 13, 14 and 15 respectively. In each case there are three factors; pore size d, filter velocity v and mass loading m, with three replications. The critical F values are determined for a significance level of 0.025 and * indicates a slight significance while ** indicates a larger (moderate) significance.

As a partial check on the analyses of variance, *SIMLIN was used to plot straight lines through the Nuc values for each of the two filter sizes (dashed lines in Figure 17) to check the significance of the regression curves. In both cases the correlation coefficients

Table 13. n-Factor analysis of variance for Nuc.

Source of variation	d. f.	M. S.	F	$F_{.025}$
d	1	4.26E-5	12.0	5.5**
v	2	7.05E-6	2.0	4.1
dv	2	3.58E-7	0.1	4.1
m	2	7.21E-6	2.0	4.1
dm	2	1.49E-5	4.2	4.1*
vm	4	5.42E-6	1.5	3.2
dvm	4	7.53E-6	2.1	3.2
Error	36	3.55E-6		
Total	53			

Means

Grand Mean = 0.00334

Factor d:

(1) = 0.00255 (2) = 0.00433

Factor v:

(1) = 0.00286 (2) = 0.00335 (3) = 0.00411

Factor m:

(1) = 0.00386 (2) = 0.00375 (3) = 0.00271

Factor d x v:

(1,1) = 0.00187 (1,2) = 0.00262 (1,3) = 0.00317

(2,1) = 0.00386 (2,2) = 0.00408 (2,3) = 0.00505

Table 14. n-Factor analysis of variance for Tube.

Source of variation	d.f.	M.S.	F	$F_{.025}$
d	1	2.17E-7	0.004	5.5
v	2	2.16E-4	3.5	4.1
dv	2	7.28E-5	1.2	4.1
m	2	4.31E-5	0.7	4.1
dm	2	1.98E-4	3.2	4.1
vm	4	1.36E-4	2.2	3.2
dvm	4	2.21E-4	3.6	3.2*
Error	36	6.13E-5		
Total	53			

Means

Grand Mean = 0.00403

Factor d:

(1) = 0.00409 (2) = 0.00397

Factor v:

(1) = 0.00286 (2) = 0.00793 (3) = 0.00130

Factor m:

(1) = 0.00511 (2) = 0.00473 (3) = 0.00226

Factor d x v:

(1, 1) = 0.00524 (1, 2) = 0.00691 (1, 3) = 0.00013

(2, 1) = 0.00048 (2, 2) = 0.00895 (2, 3) = 0.00247

Table 15. n-Factor analysis of variance for Tot.

Source of variation	d.f.	M.S.	F	$F_{.025}$
d	1	3.74E-5	0.6	5.5
v	2	1.98E-4	3.0	4.1
dv	2	6.72E-5	1.0	4.1
m	2	8.59E-5	1.3	4.1
dm	2	3.10E-4	4.8	4.1*
vm	4	1.36E-4	2.1	3.2
dvm	4	1.99E-4	3.1	3.2
Error	36	6.51E-5		
Total	53			

Means

Grand Mean = 0.00748

Factor d:

(1) = 0.00665 (2) = 0.00831

Factor v:

(1) = 0.00572 (2) = 0.01131 (3) = 0.00541

Factor m:

(1) = 0.00897 (2) = 0.00850 (3) = 0.00497

Factor d x v

(1,1) = 0.00711 (1,2) = 0.00954 (1,3) = 0.00330

(2,1) = 0.00433 (2,2) = 0.01308 (2,3) = 0.00753

are roughly 0.3 and the regressions are not significant.

The pressure drop data of Figure 18 were fitted with regression lines using *SIMLIN, resulting in the following relationships for the two filter sizes.

Filter "A": $\Delta p = -0.100 + 0.105\ v$

Filter "C": $\Delta p = -0.0291 + 0.0314\ v$

Correlation coefficients are greater than 0.99 and the regressions are highly significant in both cases. The linearities were verified for values of filter velocity in excess of 350 ft/min (178 cm/sec) using the apparatus of Figure 12.

Interpretation of Results

It is clear from Table 15 that the Tot data do not provide any positive indications that pore size, filter velocity or mass loading has any effect on penetration, and therefore efficiency, for the values

considered. This indicates that either the relationships do not exist, or there is insufficient data to determine that they do in fact exist.

It is important to recall that the Tot data are not found directly but are rather formed as the sum of two other sets of data, Nuc + Tube. Consequently, if the experimental error associated with one or both of these variables is large the experimental error for Tot will also be large. If it is large for both Nuc and Tube it will be difficult to reach any conclusions regarding the Tot data. However, if only one is large, it may be possible to further analyze the data, especially if some direct relationship between Nuc and Tube may be roughly assumed.

Observe again the Nuc and Tube data in Table 12 and consider Tables 13 and 14. Note for example that the error term (mean square) for Tube is on the order of 20 times larger than that for Nuc, and although not available from Tables 13 and 14 the variations in Tube due to replication are six times greater than that in Nuc. Note also that the average values of Nuc and Tube are roughly the same, 0.00344 and 0.00403, respectively.

Table 13 indicates that the variation in Nuc due to pore size is moderately significant, while Table 14 shows that Tube is not significant with respect to pore size. However, it does not seem reasonable that random errors for Tube should be so much larger than those for Nuc. Since Tot is the sum of Nuc + Tube, yet is still not

significant with respect to pore size, it appears that large experimental errors associated with Tube are overshadowing the significant effect of pore size on Nuc. Consequently, it seems reasonable to suggest that the difference in penetration (Tot) observed for the two pore sizes, 0.00665 for "A" and 0.00831 for "C", may in fact be significant.

It is appropriate here to comment on the negative values of penetration observed in the test data for Tube (and consequently, Tot). Very careful procedures were followed in attempting to prevent bias from entering the experiment, and evaluation indicates that these unrealistic values are due to experimental error. Consequently, it is important that the negative numbers be retained. Although the individual value may not have a real meaning, the averages will be more likely to represent the true values.

Comparison of Figure 17 with Tables 13 and 15 is instructive. For example, note in Figure 17 that for constant values of pore size the curves are functions of only filter velocity (in our case). Consequently, since v is not significant for Nuc, the slope of the two Nuc lines is not shown to be different from zero. This is verified by the results of applying *SIMLIN to the data as indicated above under Statistical Analysis. However, the two Nuc lines are in fact separate curves as indicated by the significant F-value for d in Table 13. Figures 19 and 20 also indicate that this might be the case.

Observation of the pore structures appears to show many flow passages which neck down to distances on the same order of size as the dust particles. This suggests that sieving or direct interception may play a more important role than anticipated. Consequently, efficiency (or penetration) may be a function of N_r after all. However, it must be remembered that the pores are three-dimensional and care must be used in estimating pore size from individual photographs. Note that filtration appears to be primarily a surface mechanism as expected.

Figure 21 shows that the Nuclepore filters are collecting some penetrating dust. Note that some sub-micron particles have been collected by the sections shown. However, most of the particles are in the size range from about 1 μm to 5 μm. Very few particles with diameters larger than 5 to 6 μm were observed on any of the micrographs.

Figure 18 and the associated regression analysis show that pressure drop is a linear function of filter velocity as anticipated. Further, it is assumed that the slight deviations from (o, o) are due to very small errors in the data and are insignificant. No attempt will be made to reduce the constants of proportionality to fundamental properties of the filter material. The ratio of Δp_a to Δp_c is roughly constant at 3.34 for the range of filter velocities shown.

V. DISCUSSION OF ERRORS AND CONCLUSIONS

Discussion of Errors

There are three basic categories of errors to be considered: (1) instrument errors, (2) experimental errors and (3) statistical errors.

Instrument Errors

The values of precision error associated with the various instruments used in this experiment were given previously in the section on Equipment Description and most of them are listed in Table 9. In general, the values are on the order of 2 to 3% of full scale and will not be repeated here.

However, the precision associated with the Mettler Balance has an important effect on the results and will be considered here in more detail.

Let p_u be the precision of a single measurement u. For the balance, $p_u = 0.00005$ gm. Now recall that the value of penetration is found by a simple formula involving eight measurements.

$$\phi = \frac{(Nuc_F - Nuc_T) + [(Jar_F - Jar_T) - (CJar_F - CJar_T)]}{Porex_F - Porex_T}$$

where

F designates final weight

T designates tare weight

If $z = f(x, y)$ where p_x is the precision of measurement x and p_y is the precision of measurement y with x independent of y then it is known that the precision of z is

$$p_z = \left[\left(\frac{\partial z}{\partial x} \right)^2 p_x^2 + \left(\frac{\partial z}{\partial y} \right)^2 p_y^2 \right]^{1/2}$$

From which we may obtain, for example,

$$p_{x+y} = \left[p_x^2 + p_y^2 \right]^{1/2}$$

$$p_{\frac{y}{x}} = \left(\frac{y}{x} \right) \left[\left(\frac{p_x}{x} \right)^2 + \left(\frac{p_x}{y} \right)^2 \right]^{1/2}$$

Knowing this and the average values of ϕ, $(Nuc_F - Nuc_T) + [(Jar_F - Jar_T) - (CJar_F - CJar_T)]$ and $(Porex_F - Porex_T)$ it can be shown (see Appendix G) that $p_\phi = 0.002$ gm. This is a very large error term with respect to an average value of penetration of 0.0075 gm and in future work an effort should be made to reduce it. Its effect here is to decrease our confidence in all decisions based on statistical analysis regarding the significance of any factor on penetration.

Experimental Errors

There are three main sources of experimental errors.

Inherent Variability. Inherent variability in the experimental materials results in extraneous variations which are called errors. Such properties as variations in filter pore size and sander dust particle size from run to run give rise to these errors. Such variations are not completely controllable but their effects can sometimes be minimized by careful selection of the material and proper statistical design of the experiment.

The writer believes that the large variations in the data associated with the tube washings are due to this type of error; however, no solid explanation of the variations has been found and no accurate estimate of its value is available. Considering the very small net weight of dust collected in the jars, it is possible that molecular effects are being seen due to retention of gas phase methyl alcohol in the jar pore structure during evaporation, or perhaps the washing method does not provide a complete enough removal of the dust. A check was made by successively washing the tube several times after a single run and comparing the results with both dry jars and jars containing methyl alcohol which had not been poured through the tube. Although there were some differences between groups, there were also large variations within each group

and no determination of the primary cause was evident.

Lack of Uniformity. Failure to standardize the procedure, or lack of uniformity, is the second source of experimental errors. For example, failure to wash the downstream tube with equal amounts of methyl alcohol or failure to evaporate the alcohol at equal temperatures could result in this type of error. However, due to the large variations in results already noted, extreme care was taken in performing all procedures in as uniform as manner as possible.

Bias Errors. Bias errors may also exist, such as consistently reading a scale too high or too low. Also, errors due to such things as flow leakage would result in measurements which were too high or too low consistently. This type of error is more properly termed an accuracy rather than precision error and is usually simpler to locate and correct. For example, proper calibration (of both machine and operator) should allow either of the two errors mentioned above to be adequately corrected or accounted for.

Statistical Errors

Statistical errors involving significance testing are placed in two categories. Type I errors are usually the more serious and occur when the variations due to a specified factor are determined statistically to be significant when in fact they are not. For example, the variation in Nuc data due to pore size was determined to be

significant at a significance level of 0.025. However, there is associated with this decision a probability of 0.025 [2.5%] that a Type I error exists, that is, that the variation is not significant. Type II errors are usually less serious and occur when a variation is not considered significant when in fact it is. For example, variations in the Tot data were not considered significant due to any of the factors at a significance level of 0.025. If in fact a specified factor is significant, a Type II error has occurred.

Finally, methods of reducing errors will be discussed. Of course, refinement of the experimental technique and careful selection of experimental materials should be considered. Also, selection of an appropriate statistical design and proper radomization of treatment applications are important. Perhaps the most obvious method of improving precision (reducing error) involves increasing the size of the experiment, either by adding new treatments or increasing the number of replications. Considering the data for Tot in Table 15 (see Appendix H) the size of the experiment should be increased from 54 to about 7500 if it is desired to confirm our conclusion of significant pore size effect using the Tot data.

Unfortunately, of the several hundred Porex filters originally supplied, only 60 to 75 were available which met the criteria for maintaining a low inherent variability in material properties. However, in no event were 7500 test runs possible. This points

out the importance of locating and correcting the overpowering experimental error associated with the Nuc data.

Conclusions

From the previous analyses, interpretation and discussion, the following conclusions may logically be reached.

1. The effect of pore size on penetration is significant with the following values.

Filter	Pore size d (μm)	Penetration ϕ	Efficiency $\eta = 1 - \phi$
A	19	0.0066	0.9934
C	32	0.0083	0.9917

However, this conclusion is reached by special reasoning and is not verified by the data associated solely with total penetration (Tot) at a 0.025 significance level.

2. Verification of (1) above using Tot data alone would require 7500 data points unless extraneous errors can be reduced.
3. Neither filter velocity nor mass loading is shown to be a significant factor at a 0.025 significance level.
4. Consideration of (1) and (2) above indicate that direct interception rather than inertial impaction may be the dominant filter mechanism.
5. Filtration is a surface mechanism.
6. Pressure drop is a linear function of filter velocity.

7. Pressure drop associated with the A filters is roughly 3.34 times greater than that for the C filters at the same filter velocity, over the range of velocities in the test. Consequently, it is not likely that the increased power costs would be warranted in using the A filters over the C filters, even if the variations in penetration due to pore size are significant since both efficiencies are in excess of 99% and the decrease in penetration is only 21%.

VI. SUMMARY AND RECOMMENDATIONS

Summary

A rigid porous material of sintered polyethylene powder has been developed and applied to the filtration of sander dust. A need for determining the effects of pore size, filter velocity and mass loading on efficiency (or penetration) existed and an experimental program was set up for that purpose.

The mechanisms of particle collection in filtration are well established in the literature and the effect of each mechanism in a particular filtering situation may be estimated by various proposed dimensionless parameters. Analysis of these parameters indicates that the inertial impaction mechanism involving the ratio of pore diameter to filter velocity should be dominant. Evaluation of the experimental data showed pore size to be significant, and filter velocity and mass loading to be not significant for the values of the three factors tested. The following average values of penetration resulted over all values of filter velocity and mass loading.

Filter	Pore size (μm)	Penetration
A	19	0.0066
C	32	0.0083

These results indicate that direct interception rather than inertial impaction may be the dominant filter mechanism.

Pressure drops for the two pore sizes are linear with filter velocity and the pressure differential for A is approximately 3.34 times greater than that for C at the same value of filter velocity. Consequently, to reduce the penetration from 0.0083 to 0.0066 (a 21% reduction) the pressure differential must be increased by a factor of 3.34. It is questionable whether this reduction would be worth the significantly increased power costs and fuel usage, particularly when both filters have efficiencies exceeding 99%.

A severe limitation in the results is caused by large unexplained variations in certain of the data. Further work in eliminating this problem is needed so that more concrete conclusions may be reached.

Recommendations

The following specific recommendations are made regarding future work associated with this study.

1. Locate and eliminate the large extraneous experimental errors.
2. Incorporate filters with larger average pore sizes (up to 100 μm).
3. Extend the scope to include the effects of filter cake buildup.
4. Increase the filter surface area to increase dust holding capabilities.
5. Increase the size of the experiment.

BIBLIOGRAPHY

1. American Petroleum Institute, "Removal of particulate Matter from gaseous wastes: filtration," New York, 1961. 56 p.

2. American Meter Company. "Orifice meter constants," Handbook E-2, Revised to conform with A. G. A. Report No. 3, American Meter Company, Inc., 1955. 114 p.

3. American Society for Testing and Materials. "Standard method of test for maximum pore diameter and permeability of rigid porous filters for laboratory use." Reprint from 1965 book of ASTM Standards, Part 30. ASTM Designation: E 128-61. Adopted 1961. p. 826-829.

4. American Society for Testing and Materials. "Tentative method of test for pore size characteristics of membrane filters for use with aerospace fluids," Part II. 1968 Book of ASTM Standards, Part 18. ASTM Designation: D 2499 - 66T. p. 628-634.

5. American Society for Testing and Materials. "Symposium on particle size measurement," Presented at the Fifty-Fifth Annual Meeting, N. Y., June 25, 1952.

6. Anderson, G. E. "Filter pore size - mean-flow pore test," Association of American Railroads, Society of Automotive Engineers, "Fuel filter test methods," Volume 1, Jan. 1961. p. 30-33.

7. Boubel, R. W. Consulting Engineer. "Particulate emissions," Unpublished Report for Timber Products Company, Medford, Oregon, Dated November 17, 1971.

8. Boubel, R. W. Consulting Engineer. "Particulate emissions," Unpublished Report for White City Plywood, White City, Oregon, Dated Oct. 7, 1971.

9. Boubel, R. W. Consulting Engineer. "Rader filter system analysis," Unpublished Report issued to the Weyerhaeuser Company, Longview, Wash. Feb. 11, 1971.

10. Cadle, R. D. "Particle size," Reinhold Publishing Company, New York, 1965. 382 p.

11. Carls, E. L. and N. M. Levitz. "Blowback of sintered-metal filters: A review of tests and operating experience," Argonne National Laboratory Report No. ANL-7392, 1968. 30 p.

12. Chen, C. Y. "Filtration of aerosols by fibrous media," Chemical Reviews, 55, 1955. p. 595-623.

13. Clark, J. Personal phone conversation, Vice President of Rader Companies Incorporated, 2400 Poplar Ave., Memphis, Tenn. July 9, 1973.

14. Davies, C. N. (Ed.). "Aerosol science," Academic Press, London, 1966. 468 p.

15. Farnworth, W. Personal discussion, Rader Pneumatics, Portland, Oregon. Aug. 31, 1971.

16. First, M. W. and L. Silverman. "Predicting the performance of cleanable industrial fabric filters," Journal of the Air Pollution Control Association, 13 (12), December 1963. p. 581-586.

17. GCA Corporation. "Handbook of fabric filter technology. Volume I. Fabric Filter Systems Study." Contract No. CPA-22-69-38, For the National Air Pollution Control Administration, 1970. 649 p.

18. Heating, Piping and Air Conditioning. "Know rating methods when selecting air cleaning devices," January 1962. p. 181-185. No Author cited.

19. Holt, P. F. and D. K. Young. "A dust-feed mechanism suitable for fibrous dust," Annals of Occupational Hygiene, 2, 1960. p. 249-256.

20. Isaacson, R. E. Personal letter to C. M. Anderson, Weyerhaeuser Company, Springfield, Oregon. Aug. 19, 1971.

21. Junge, D. C. Personal phone conversation, Senior Research Engineer, Environmental Research Division, Weyerhaeuser Company, Longview, Wash. Dec. 19, 1972.

22. Kane, L. J. et al. "Porous stainless steel filters for removing dust from hot gases." Bureau of Mines Report No. 5842, 1961. 18 p.

23. Kraus, M. N. "Pneumatic conveying: Equipment and controls," Chemical Engineering, May 10, 1965. p. 149-164.

24. Kraus, M. N. "Pneumatic conveying: General considerations," Chemical Engineering, April 12, 1965. p. 167-182.

25. Los Angeles County Air Pollution Control District. "Air pollution source testing manual," 434 South San Pedro St., Los Angeles, California, 1963. 179 p.

26. Machacova, J. et al. "Analytical methods for determination of aerosols by means of membrane ultrafilters. XV. Hydrodynamical properties of membrane and nuclear pore filters." Collection of Chechoslovak Chemical Communications (Prague), 35, 1970. p. 2087-2099.

27. May, J. W. "Efficiency testing and applications of air filters," Heating, Piping and Air Conditioning, March 1969. p. 140-143.

28. Midwest Research Institute. "Particulate pollutant systems study. Volume I - Mass emissions," Contract No. CPA 22-69-104, For the Environmental Protection Agency, 1971. 372 p.

29. Midwest Research Institute. "Particulate pollutant systems study. Volume III - Handbook of emission properties," Contract No. CPA 22-69-104, For the Environmental Protection Agency, 1971. 629 p.

30. Nuclepore Corporation, Pleasanton, California. Brochure GEA - 8342 4/71 (15 M). April 1971.

31. Pall, D. B. "Filtration of fluid catalyst fines from effluent gases," Industrial and Engineering Chemistry, 45, 1953. p. 1197-1202.

32. Pich, J. "Impaction of aerosol particles in the neighborhood of a circular hole," Collection of Chechoslovak Chemical Communications (Prague), 29, 1964. p. 2223-2227.

33. Porex Materials Corporation. Fairborn, Georgia. Untitled literature on POR·X material. 1971.

34. Porvair Limited. King's Lynn Norfolk, England. "Technical data sheet (provisional draft): VYON."

35. Quakenbush, D. W. "Plugged tubular filters at Coos Bay," Project 040-0148, Weyerhaeuser Company, Longview, Washington. September 27, 1971.

36. Ranz, W. E. and J. B. Wong. "Impaction of dust and smoke particles on surface and body collectors," Industrial and Engineering Chemistry, 44 (6), June 1952. p. 1371-1381.

37. Rootare, H. M. "A short literature review of mercury porosimetry as a method of measuring pore-size distributions in porous materials, and a discussion of possible sources of errors in the method," Aminco Reprint 439, American Instrument Company, Silver Spring, Maryland. 8 p.

38. Scheidegger, A. E. "The physics of flow through porous media," The Macmillan Company, New York, 1960. 313 p.

39. Spurny, K. and G. Madelaine. "Analytical methods for determination of aerosols by means of membrane ultrafilters. XIX. Efficiency measurement of nuclepore filters by means of latex aerosols." Collection of Czechoslovak Chemical Communications (Prague), 36, 1971. p. 2857-2866.

40. Spurny, K. R. and J. P. Lodge, Jr. "Analytical methods for determination of aerosols by means of membrane ultrafilters. XI. Structural and filtration properties of nuclear pore filters." Collection of Czechoslovak Chemical Communications (Prague), 33, 1968. p. 3679-3693.

41. Spurny, K. and J. P. Lodge, Jr. "Analytical methods for determination of aerosols by means of membrane ultrafilters. XII. Filtration mechanisms of pore filters studied by means of electron microscopy." Collection of Czechoslovak Chemical Communications (Prague), 33, 1968. p. 3931-3939.

42. Spurny, K. and J. Pich. "Analytical methods for determination of aerosols with help of membrane ultrafilters. VI. On the mechanisms of membrane ultrafilter action." Collection of Czechoslovak Chemical Communications (Prague), 30, 1965. p. 2886-2894.

43. Spurny, K. and J. Pich. "Analytical methods for determination of aerosols by means of membrane ultrafilters. VII. Diffusion and impaction precipitation of aerosol particles by membrane ultrafilters." Collection of Czechoslovak Chemical Communications (Prague), 30, 1965. p. 2276-2287.

44. Spurny, K. R. et al. "Aerosol filtration by means of Nuclepore filters: structural and filtration properties." Environmental Science and Technology, 3 (5), May 1969, p. 453-464.

45. Strauss, H. J. "The present situation in the field of air filter testing," Staub:Reinhalt der Luft (in english), Oct. 1968. p. 1-6.

46. Volk, W. "Applied statistics for engineers." 2nd. ed. McGraw-Hill Book Company, New York, 1969. 415 p.

APPENDICES

APPENDIX A

THE CAPILLARY RISE EQUATION

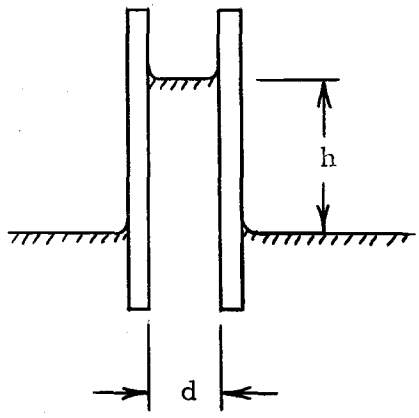

ρ_L = Liquid density

S = Liquid surface tension

θ = Liquid contact angle

F = Surface tension force

g = Gravitational acceleration

W = Column liquid weight

$$F = \pi d S \cos\theta$$

$$W = \frac{\pi}{4} d^2 h \rho g$$

For equilibrium $F = W$

$$\pi d S \cos\theta = \frac{\pi}{4} d^2 h \rho g$$

$$\frac{4S \cos\theta}{d} = \rho g h$$

For complete wetting $\theta = 0$, $\cos\theta = 1$

$$\rho g h = \frac{4S}{d}$$

APPENDIX B

CALCULATION OF FILTRATION MECHANISM PARAMETERS

I. Collector Model

$$R = \frac{D_p}{D_c} \qquad I = \frac{C_s \rho_p D_p^2 v_o}{18 \mu D_c} \qquad G = \frac{C_s \rho_p g D_p^2}{18 \mu v_o}$$

where

D_p = Particle diameter = $\begin{matrix} 8.7\ \mu m \text{ count mean} \\ 22\ \mu m \text{ weight mean} \end{matrix}$

D_c = Collector diameter = 40 and 70 μm

C_s = Slip correction factor = 1

ρ_p = Particle density = 0.625 gm/cm^3

v_o = Free stream velocity = 7.6 and 12.7 cm/sec

μ = Air vicosity = 185 (10)$^{-6}$ gm/sec-cm

g = Gravitational acceleration = 980 cm/sec^2

	Range for count mean size (D_p = 8.7 μm)	Range for weight mean size (D_p = 22 μm)
R	0.12 to 0.22	0.31 to 0.55
I	0.13 to 0.30	1.0 to 2.3
G	0.01 to 0.015	0.07 to 0.11

II. Pore Model

$$N_R = \frac{D_p}{d} \qquad N_I = \frac{\rho_p D_p^2 v_o}{9 \mu d p} \qquad N_G = \frac{LP \rho_p g D_p^2}{6 d \mu v_o}$$

where

d = Pore diameter = 19 and 32 μm

P = Porosity = 0.4

L = Pore length = 0.076 cm

	Range for count mean size (D_p = 8.7 μm)	Range for weight mean size (D_p = 22 μm)
N_R	0.27 to 0.46	0.68 to 1.2
N_I	1.7 to 4.7	10.8 to 30.2
N_G	0.31 to 0.88	2.0 to 5.6

APPENDIX C

PORE DIAMETER AND DISTANCE BETWEEN PORES AS A FUNCTION OF COLLECTOR SIZE

I. Plane Triangular Packing

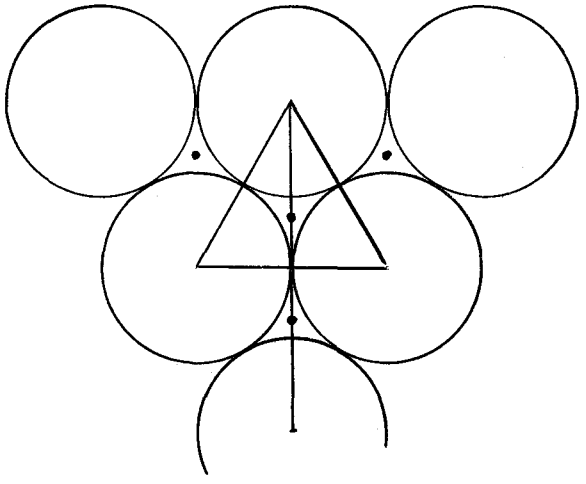

D_c = Collector diameter

x = Triangle base

y = Triangle height

z = Distance between adjacent pores

A_t = Triangle area

A_d = Pore cross-sectional area

d = Equivalent pore diameter

$$A_t = xy = D_c \left(\frac{\sqrt{3}}{2}\right) D_c = \frac{\sqrt{3}}{2} D_c^2$$

$$A_d = A_t - 3\left(\frac{1}{6}\right)\left(\frac{\pi}{4}\right) D_c^2 = \left[\frac{\sqrt{3}}{2} - \frac{\pi}{8}\right] D_c^2$$

$$\frac{\pi}{4} d^2 = A_d = \left[\frac{\sqrt{3}}{2} - \frac{\pi}{8}\right] D_c^2$$

$$d = \left[\frac{2\sqrt{3}}{\pi} - \frac{1}{2}\right]^{1/2} D_c$$

$$z = 2\left(\frac{y}{3}\right) = \frac{2}{3}\left(\frac{\sqrt{3}}{2}\right) D_c$$

$$z = \frac{\sqrt{3}}{3} D_c$$

II. Plane Quadrangular Packing

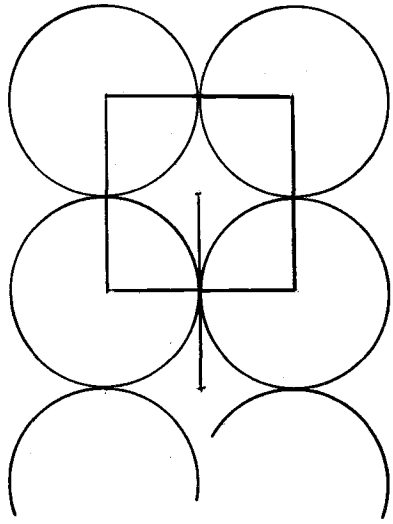

D_c = Collector diameter

x = Square side

z = Distance between adjacent pores

A_s = Square area

A_d = Pore cross-sectional area

d = Equivalent pore diameter

$$A_s = x^2 = D_c^2$$

$$A_d = A_s - 4\left(\frac{1}{4}\right)\left(\frac{\pi}{4}\right) D_c^2 = \left(1 - \frac{\pi}{4}\right) D_c^2$$

$$\frac{\pi}{4} d^2 = A_d = \left(1 - \frac{\pi}{4}\right) D_c^2$$

$$d = \left(\frac{4}{\pi} - 1\right)^{1/2} D_c$$

$$z = 2\left(\frac{D_c}{2}\right)$$

$$z = D_c$$

APPENDIX D

CALCULATION OF NUCLEPORE EFFICIENCY

From Spurny and Lodge (40), Spurny et al. (44) and Spurny and Madelaine ( )

$$\eta = e_i + (1 + e_i)\left[e_d + e_R\,\gamma^{(1-N_R)}\right]$$

where

$$e_i = \frac{2e_i'}{1+\beta} - \left(\frac{e_i'}{1+\beta}\right)^2$$

$$e_i' = 2\,N_I\sqrt{\beta} + 2\,N_I^2\,\beta\,\exp\left[-\frac{1}{N_I\sqrt{\beta}}\right] - 2\,N_I^2\,\beta$$

$$\beta = \frac{\sqrt{P}}{1-\sqrt{P}}$$

$$N_I = \frac{\rho_p\,D_p^2\,v_o}{9\,\mu\,d\,P}$$

$$e_d = 1 - 0.82\exp\left[-3.66\,N_D\right] - 0.098\exp\left[-22.3\,N_D\right]$$

$$- 0.033\exp\left[-57\,N_D\right] - 0.016\left[-108\,N_D\right]$$

$$N_D = \frac{L\,\ell\,P}{4d^2\,v_o}$$

$$e_R = N_R\,(2 - N_R)$$

$$N_R = \frac{D_p}{d}$$

η = Efficiency (mass = count for single size)

ℓ = Particle diffusion constant = $3(10)^{-7}$ cm^2/sec for 1 μm particle

d = Pore diameter = 3 μm

D_p = Particle diameter = 1 μm

L = Pore length = filter thickness = 10 μm

v_o = Free stream velocity = filter velocity = 30 cm/sec

P = Porosity = 0.15

ρ_p = Particle density = 0.625 gm/cm^3

μ = Air vicosity = $185(10)^{-6}$ gm/sec-cm

γ = Constant = 0.63

$$\beta = \frac{\sqrt{0.15}}{1 - \sqrt{0.15}} = 0.63 \qquad \sqrt{\beta} = 0.8$$

$$N_I = \frac{0.625(1)(10)^{-8}(30)}{9(185)(10)^{-6}(3)(10)^{-4}(0.15)} = 2.5$$

$e_i' = 0.9$ $\qquad$ $e_i = 0.8$

$$N_D = \frac{10(10)^{-4}(3)(10)^{-7}(0.15)}{9(10)^{-8}(30)(4)} = 4.2(10)^{-6} \qquad e_D = 0.033$$

$$N_R = \frac{1}{3} = 0.33 \qquad e_R = 0.56$$

$$\eta = 0.89$$

APPENDIX E

SIMPLIFICATION OF MACHACOVA'S EQUATION FOR FLOW THROUGH MEMBRANE AND NUCLEPORE FILTERS

From Machacova (26)

$$\Delta p = p_1 - \left[p_1^2 - \frac{K_2 \mu L v_o p_1}{P d^2} \right]^{1/2}$$

where

Δp = Differential pressure

p_1 = Upstream absolute pressure

K_2 = Constant

μ = Air viscosity

L = Pore length

v_o = Free stream velocity

P = Porosity

d = Pore diameter

Let p_2 = Downstream absolute pressure

$$\Delta p = p_1 - p_2$$

$$p_2 = \left[p_1^2 - \frac{K_2 \mu L v_o p_1}{P d^2} \right]^{1/2}$$

$$p_2^2 = p_1^2 - \frac{K_2 \mu L v_o p_1}{P d^2}$$

$$p_1^2 - p_2^2 = (p_1 - p_2)(p_1 + p_2) = \frac{K_2 \mu L v_o p_1}{P d^2}$$

$$\Delta p \left[\frac{p_1 + p_2}{p_1} \right] = \frac{K_2 \mu L v_o}{P d^2}$$

For $\Delta p << p_1$, $\frac{p_1 + p_2}{p_1} \simeq 2$

$$\Delta p = \frac{K_2 \mu L v_o}{2 P d^2}$$

If $Q = A v_o$

where

Q = Volumetric flow rate

A = Cross-sectional area

$$\Delta p = \frac{K_2 \mu L Q}{2 P A d^2}$$

$$Q = \left[\frac{P d^2 A}{2 K_2 \mu L} \right] \Delta p$$

$$Q = \left[\frac{k_2 A}{\mu L} \right] \Delta p$$

where

$$k_2 = \frac{P d^2}{2 K_2}$$

APPENDIX F

ESTIMATION OF TEST SANDER DUST WEIGHT MEAN SIZE

Count data: Count mean size $D_{pc} = 8.7\ \mu m$
Geometric deviation $\sigma_{pc} = 1.8$
Range (1 to 99%) $H = 2.2$ to $35\ \mu m$

% of Range	Fraction enclosed (δ)	Upper class mark (D_c)	Ave. size ($\overline{D}_c$)	$\delta \overline{D}_c^3$	Cum. %
1		2.2			
10	(0.10)	4.1	3.1	2.9	0.1
20	0.10	5.3	4.7	10.3	0.5
30	0.10	6.3	5.8	19.5	1.2
40	0.10	7.5	6.9	32.9	2.5
50	0.10	8.7	8.1	53.1	4.5
60	0.10	10.0	9.4	83.1	7.6
70	0.10	12.0	11.0	133.0	12.6
75	0.05	13.0	12.5	98.0	16.3
80	0.05	14.5	13.8	131.0	21.3
85	0.05	16.0	15.3	179.0	28.0
89	0.04	18.0	17.0	196.0	35.4
92	0.03	20.0	19.0	206.0	43.2
94	0.02	22.0	21.0	185.0	50.2 ←
96	0.02	24.5	23.3	253.0	59.7
98	0.02	29.5	27.0	394.0	74.6
99	(0.02)	35.0	32.3	674.0	100.0
				2650.0	

Estimate weight mean size $D_{pm} = 22\ \mu m$

APPENDIX G

ESTIMATION OF PENETRATION PRECISION

$$\phi = \frac{(Nuc_F - Nuc_T) + [(Jar_F - Jar_T) - (CJar_F - CJar_T)]}{Porex_F - Porex_T}$$

Where

F indicates final weight

T indicates tare weight

and the precision of each individual measurement u is p_u.

It is known that, for any x and y where x is independent of y,

$$p_{x+y} = [p_x^2 + p_y^2]^{1/2}$$

$$p_{\frac{y}{x}} = \left(\frac{y}{x}\right)\left[\left(\frac{p_x}{x}\right)^2 + \left(\frac{p_x}{y}\right)^2\right]^{1/2}$$

In the equation for ϕ above let y be the numerator and x the denominator. Then, for $\phi = 0.0075$, $x = 0.06$ gm, $y = 0.00045$ gm, and $p_u = 0.00005$ gm,

$$p_y = [6\, p_u^2]^{1/2} = 0.000122 \text{ gm}$$

$$p_x = [2\, p_u^2]^{1/2} = 0.000071 \text{ gm}$$

So

$$p_{\phi} = p_{\underset{x}{y}} = \phi\left[\left(\frac{p_x}{x}\right)^2 + \left(\frac{p_y}{y}\right)^2\right]^{1/2}$$

$$p_{\phi} = 0.002$$

APPENDIX H

ESTIMATION OF DESIRED EXPERIMENT SIZE

The value of the t-distribution for a difference in means is given by

$$t_{\frac{\alpha}{2}} = \frac{\bar{d} - \mu_d}{\sigma_d}$$

Where

$$\bar{d} = \bar{x}_1 - \bar{x}_2$$

$$\mu_d = \mu_1 - \mu_2$$

$$\sigma_d = \left[\frac{2\sigma_x^2}{\frac{n}{2}} \right]^{1/2}$$

n = total sample size

so

$$\mu_d = \bar{d} \pm t_d \left[\frac{4\sigma_x^2}{n} \right]^{1/2}$$

and the confidence interval on d is

$$CI_d = 2 t_{\frac{\alpha}{2}} \left[\frac{4\sigma_x^2}{n} \right]^{1/2}$$

If we choose

$$\alpha = 0.025$$

$CI_d = 0.001$ gm

$\sigma_x^2 =$ Tot error term $= 9.32\,(10)^{-5}$ gm^2 (see Table 15)

Then from a table of the t-distribution

$$t_{\frac{\alpha}{2}} = 2.24 \text{ and}$$

$$0.001 = 2\,(2.24)\left[\frac{4(9.32)\,(10)^{-5}}{n}\right]^{1/2}$$

or

$$n = 4\,(9.32)\,(10)^{-5}\left[\frac{2\,(2.24)}{0.001}\right]^{2}$$

$$n = 7500$$